Xenolith Formation and the Development of Basaltic Volcanic Conduits During the 1975 Tolbachik Eruptions, Kamchatka, with Implications for Volcanic Hazards Assessments at Yucca Mountain, Nevada

Philip Doubik[a], Brittain E. Hill[b1]

[a]*Department of Geology, State University of New York, Buffalo, NY 14260 U.S.A.*
[b]*Center for Nuclear Waste Regulatory Analyses, Southwest Research Institute, 6220 Culebra Rd., San Antonio, TX 78238-5166 U.S.A.*

ABSTRACT

Xenoliths in pyroclastic fall deposits from the 1975 Tolbachik eruption provide detailed information about the timing and development of subsurface conduits associated with basaltic cinder cone eruptions. The two largest vents from the 1975 Tolbachik eruption contain xenoliths derived from magmatic and hydromagmatic processes, which can be correlated with observed styles of eruption activity. Although many basaltic eruptions progress from early hydromagmatic activity to late magmatic activity, transient hydromagmatic events occurred relatively late in the 1975 Tolbachik eruption sequence. Magmatic fall deposits contain 0.01–0.3 volume percent xenoliths derived from <3-km-deep rocks, which can be derived from cylindrical conduits 6–15 m wide and 1.7–2.8 km deep. Eruption periods that supported the highest tephra columns (i.e., droplet flow regime) produced few of these xenoliths. Most of these xenoliths were derived from periods with relatively lower tephra columns and active lava flows (i.e., annular 2-phase flow). Several periods of decreased eruptive activity resulted in inflow of deep (>500 m) groundwater into the dry-out zone around the conduit, disrupting and ejecting 10^5–10^6 m^3 of wall-rock through hydromagmatic processes. Cylindrical conduits widened to 8–48 m to accommodate these volumes. Hydromagmatic falls contain 60–75 volume percent of highly fragmented xenoliths, with juvenile clasts displaying obvious magma-water interaction features. During the largest hydromagmatic event, unusual breccia-bombs formed that contain a wide range of fresh and pyrometamorphic xenoliths suspended in a quenched basaltic matrix. Following the main hydromagmatic events, magmatic eruptions continued for 30 days. Larger silicic eruptions may have transient hydromagmatic events in response to conduit flow dynamics above the magma fragmentation depth. Hydromagmatic activity during the 1975 Tolbachik eruption occurred below likely fragmentation depths for a basalt containing 2.2 weight percent magmatic water and is likely related to conduit-wall collapse rather than variations in conduit-flow pressure. Volcanic hazards assessments for the proposed high-level

---

[1]Corresponding author. Fax: 210-522-5155. E-mail: bhill@swri.edu
Keywords: xenolith, Tolbachik, Kamchatka, eruption, conduit, hydromagmatic

radioactive waste repository site at Yucca Mountain, Nevada, need to consider the dimensions of basaltic subvolcanic conduits to evaluate the amount of waste that can be potentially ejected during a future volcanic event. The 1975 Tolbachik volcanoes are reasonably analogous to Quaternary basaltic volcanoes in the Yucca Mountain region and can guide interpretations of the poorly preserved deposits in the Yucca Mountain region. The youngest basaltic volcanoes in the Yucca Mountain region have cone deposits characterized by elevated xenolith abundances and distinctive xenolith breccia-bombs, remarkably similar to 1975 Tolbachik deposits. Extrapolation of 1975 Tolbachik data suggests conduits for some Yucca Mountain basaltic volcanoes may have widened on the order of 50 m in response to late-stage hydromagmatic events. Volcanic hazards assessments for the proposed repository site need to consider that future basaltic eruptions appear capable of forming conduits with diameters on the order of 50 m at proposed repository depths.

1 INTRODUCTION

Basaltic cinder cones typically represent the lower end of hazards associated with volcanic eruptions. Relative to silicic composite volcanoes, the small volumes of ejecta and limited dispersal capabilities of cinder cones restrict most acute hazards to within several kilometers of the vent. Tephra falls from basaltic cinder cones, however, can extend dekakilometers downwind and adversely affect agricultural and engineered systems. A proposed high-level radioactive waste repository site at Yucca Mountain, Nevada, is located in an area where the bounding probability of a new basaltic cinder cone forming through the repository is 10^{-3} during a 10^4-year post-closure period (e.g., Connor and Hill, 1995; Connor et al., 1996). Several of the <1 Ma cinder cones in the Yucca Mountain region show evidence of "violent strombolian" (Walker, 1973) eruptions, which likely supported tephra columns at least several kilometers high and dispersed tephra dekakilometers downwind (e.g., Jarzemba, 1997; Hill et al., 1998). A critical process in evaluating potential volcanic hazards for the Yucca Mountain repository is determining the amount of subsurface (300-m deep) rock that potentially can be entrained and ejected during a future basaltic cinder cone eruption. Although the free-surface effects of a large tunnel network likely will affect how ascending magma interacts with the surrounding rock, data from historically active volcanoes can indicate how much shallow subsurface rock can be disrupted during a basaltic cinder cone eruption. Several studies have examined xenolith formation in basaltic phreatomagmatic and spatter-cone eruptions (e.g., Wohletz, 1983; Valentine and Groves, 1996), however, no studies have examined xenolith formation in violent strombolian eruptions.

The 1975 Tolbachik eruption is an excellent example of a basaltic violent strombolian eruption. Tephra column heights ranged from 2–12 km during 70 days of activity, with 10 cm of tephra deposited 20 km downwind (Budnikov et al., 1983). An unusual feature of the 1975 Tolbachik eruption was several short periods of activity when most of the ejecta was extensively fragmented wall-rock. Along with proximal xenolith blocks, xenolith-rich ash was distributed as distinct stratigraphic beds in the tephra deposits. Significant conduit widening is necessarily associated with significant xenolith production. If this xenolith formation process were to occur at Yucca Mountain cinder cones, volcanic hazards assessments would need to consider the area disrupted by a basaltic conduit on the scale of dekameters rather than meters.

Ia Geologic Setting

The 1975 Tolbachik eruption continued a 10,000-year episode of basaltic cinder cone activity extending south from Plosky and Ostry Tolbachik volcanoes, Kamchatka (Figure 1). At least 150 Holocene basaltic cinder cones and fissure vents cover 900 km^2 of the Tolbachik Middle–Upper Pleistocene mafic platform, which formed in a NE-trending intra-arc graben with about 1 km vertical displacement (Erlich, 1973). Vents in the Holocene Tolbachik cinder cone field form prominent NNE-trending alignments that parallel the major structural features of the graben, with most vents concentrated in a 3–4-km-wide axial zone (Figure 1). The 1975 eruption continues activity along a prominent NNE-trending alignment of cinder cones and fissure vents, which last erupted 190 yr B.P. (Braytseva et al., 1983). Other historical activity in the Tolbachik system includes multiple explosive eruptions from the summit crater of Plosky Tolbachik and a flank eruption in 1941. Basalt petrogenesis in the Tolbachik region has changed significantly since 2 ka. Between 2–10 ka, high-Al_2O_3 "megaplagiophyric" basalts constituted 90 volume percent of the 80 km^3 erupted from Plosky Tolbachik and the surrounding cinder cone field (Melekestzev et al., 1970). High-MgO basalt comprises 35 volume percent of the 40 km^3 erupted in the region since 2 ka (Braytseva et al., 1983; Melekestzev et al., 1970), including the 1941 and 1975 eruptions (Volynets et al., 1983).

Regional variations in shallow crustal stratigraphy constrain the sources of xenoliths and eruptive processes in the Tolbachik area. Interbedded Holocene lavas and tephra form the upper 200–300 m of the Tolbachik section and overlie a 1000-m-thick section of Middle–Upper Pleistocene megaplagiophyric platform basalts (Erlich, 1973). The base of the volcanic section is well resolved by seismic studies (Balesta et al., 1983, 1984). Platform basalts grade downward into interbedded sedimentary rocks of the Neogene Shapinskaya formation (Khramov and Salin, 1966). The upper Shapinskaya formation is dominated by volcanically derived sandstones and siltstones with interbedded lavas and tuffs, which were likely deposited in a fore-arc basin (Shanzer, 1979; Shanster, 1983). Fore-arc sediments rest upon volcanically derived sandstones and siltstones of the lower Shapinskaya formation, which were deposited in a littoral marine environment (Shanster, 1983). The Shapinskaya formation is 3.5–4 km thick (Khramov and Salin, 1966; Balesta et al., 1983) and was deposited upon a Paleogene flysch sequence that formed when a Cretaceous and older crustal section was accreted to Kamchatka (e.g., Geist et al., 1994). Resistivity studies (Balesta et al., 1984) and the distributions of springs indicate depth to the water table of 500–800 m beneath the site of the 1975 Tolbachik eruption.

2 SUMMARY OF THE 1975 TOLBACHIK ERUPTION

The chronology of the 1975 Tolbachik eruption is summarized to present the sequence and character of events that typically may accompany a basaltic cinder cone eruption. Information in this section is compiled from Budnikov et al. (1983), Connor et al. (1997), Doubik et al. (1995), Faberov (1983), Fedotov (1983), Fedotov et al. (1976; 1984; 1991), Jayaweera et al. (1976), Maleyev and Vande-Kirkov (1983), Tokarev (1978, 1983), and eyewitness accounts (Yu. Doubik, A. Ovsyannikov and V. Shapar).

The 1975 eruption was heralded by a swarm of more than 300 earthquakes near the eruption site, which began on 27 June 1975. Depth of the epicenters ranged mainly from 2 to 20 km and decreased over the next 7 days. Sporadic ash and gas emissions occurred at the summit caldera of nearby Plosky Tolbachik (Figure 1) on 28 June and continued to 7 July 1975. Intense earthquake activity continued until 4 July, when activity rapidly declined over a 24-hour period. On 6 July, a 300-m-long fissure trending 320°opened at the site of Cone 1 (Figure 2) and formed three small cinder and spatter cones. Eruption products consisted of high-MgO basalt, similar in composition to basalt erupted in 1941 (Figure 2). By 7 July, activity had coalesced into a single vent, Cone 1, and eruption intensity began to increase from small pulsed events into sustained convective discharge. Column heights averaged 5–8 km by 10 July, with the visible eruption plume extending 200–500 km to the south. Eruption explosivity generally increased with time and the ash column occasionally rose to 18 km, although altitudes of 6–10 km were more typical. During the major part of the Cone 1 eruption, seismicity remained at a low level of activity with a few events at depths of 0–10 km. Eruption activity continued essentially unchanged until 23 July, when pauses in the eruption of several seconds to hours began. The first lava was erupted from a bocca immediately south of Cone 1 on 29 July (Figure 2), accompanied by a marked decrease in eruption explosivity and numerous pauses in activity. A second lava flow was erupted from a bocca on the north flank of Cone 1 on 2 August 1975, when convective column heights were 2–3 km. Short pauses in the eruption of tephra continued throughout this interval, however, lava flows continued to emanate from boccas during these pauses. Seismic activity increased between 2 and 9 August, with activity concentrated immediately north of Cone 1 and broadly extending to the summit of Plosky Tolbachik.

A 9-hour pause in the tephra eruption occurred late in the evening of 7 August. Although the eruption of tephra recommenced at 8:18 on 8 August, lava from the southern Cone 1 bocca ceased.

Following a several hour pause in the eruption during the late afternoon of 8 August, the character of the tephra eruption changed dramatically. Instead of wholly juvenile basaltic magma, for 12 hours the ejecta consisted of dominantly pulverized subsurface rock intermixed with juvenile magma. This period of the eruption is referred to as the white-ash event (WA-1), representing brecciation and dispersal of several million cubic meters of relatively shallow subsurface rock. Although most of the white-ash eruption occurred after nightfall, during this time the WA-1 event was marked by unusually loud jetlike sounds that came from Cone 1. Formation of WA-1 marked the end of the Cone 1 eruption on 9 August, 1975.

Although most observers believed the eruption had ceased with the end of activity at Cone 1, 13 hours later a second, 400-m-long fissure opened 800 m north of Cone 1 late on 9 August 1975. Cone 2 began to form over that fissure with the eruption of both tephra and lava from a rapidly centralized vent. The Cone 2 eruption continued through 15 September, with several lava boccas formed at the base and vicinity of the main vent. A third cone, Cone 3, formed 750 m north of Cone 2 on 16 August and erupted simultaneously with Cone 2 until 25 August. All activity ceased at Cone 2 on 15 September 1975. Eruptions from Cones 2 and 3 were less explosive than Cone 1, with convective column heights generally less than 4 km and a visible eruption plume extending to <300 km of the vent. Several comparatively small white-ash events also occurred during the Cone 2 eruption, generally in association with formation of larger boccas. The largest of the Cone 2 white-ash events (WA-2) occurred on 16 August during the formation of Cone 3.

Following a 3-day hiatus in activity, a new cone formed 10.5 km south of Cone 2. In contrast to Cones 1–3, the Southern Cone erupted high-Al_2O_3 basalt that had a minor high-MgO component for the first 2 weeks of the eruption. Significant amounts of high-Al_2O_3 basalt also were mixed into the erupting magma system during the last week of activity at Cone 2. Activity at Southern Cone was relatively low energy and formed a spatter cone with only locally distributed ash. Most of Southern Cone and associated lavas formed during late 1975, but a low level of activity continued to December 10, 1976. Activity at Southern Cone is not examined in this report owing to the marked change in composition, eruption style, and large spatial separation from the Cones 1–3 deposits.

3 PETROLOGY OF PYROCLASTIC DEPOSITS

3a Stratigraphy

Basaltic fall deposits from Cones 1–3 cover an area of 240 km^2 to a depth of 10 cm (Figure 1). Using the isopach map from Budnikov et al. (1983), computer-assisted cartography, and the two-slope line method of Fierstein and Nathenson (1992), we calculate a proximal volume of 0.22 km^3 for the Cones 1–3 falls. Fall-deposit volumes of around 0.2 km^3 were calculated by Budnikov et al. (1983) out to 60 km from the 10-cm isopach, giving a total fall-deposit volume of 0.42 km^3. Using a deposit density of 1200 kg m^{-3} and a calculated (Lange and Carmichael, 1987; Lange, 1994) basalt density of 2600 kg m^{-3}, Cones 1–3 erupted 0.19 km^3 dense rock equivalent (DRE) of basalt as tephra fall. In comparison, 0.24 km^3 DRE of lavas (density of 2400 kg m^{-3}) erupted from Cones 1–3 and 0.17 km^3 DRE erupted as cinder cones (density of 2200 kg m^{-3}).

Studied fall-deposit sections are 0.5–1.5-m thick and contain 15–20 internal units defined by grain-size variations. Cone 1 deposits are thickest in western exposures and constitute 55 percent of the total 1975 Tolbachik fall deposit. Xenolith-rich white ash beds form distinct stratigraphic horizons internal to the 1975 Tolbachik fall deposits. WA-1 was deposited primarily west of the main vents and has a reported volume of 7×10^6 m^3 (Budnikov et al., 1983), which is consistent with a volume of 6×10^6 m^3 calculated from field measurements (Figure 2). Tops of Cone 1 deposits are clearly marked by WA-1 beds in western deposits. WA-1 beds are absent east of Cone 1, where the tops of Cone 1 deposits are recognized by reduction in grain size, increase of dendritic forms to pyroclasts, and increase in degree of pyroclast vesiculation. Although several white-ash events occurred during the eruption of Cones 2 and 3, only one event (WA-2) created a mappable deposit. The thin WA-2 deposit has an estimated volume of 1×10^5 m^3 (Figure 2).

The WA-1 deposit is plane-parallel bedded and has a well-developed internal stratigraphy. Three main layers (WA-1B, WA-1C, and WA-1D) are recognizable in all sampled sections based on variations in grain-size and sorting characteristics (Figure 3). Layer WA-1B is clast supported, ranges in thickness from 1.5–9 cm, and consists of lapilli rimmed with light-colored fine ash. Ash rinds obscure the original irregular shapes of large clasts and give a false appearance of rounded accretionary lapilli. The lower contact of layer WA-1B with the latest tephra of Cone 1 is sharp and not eroded. Layer WA-1B grades

upward into layer WA-1C, which consists of subequal proportions of lapilli and ash, is matrix supported, and varies in thickness from 1–7 cm in the studied sections. Layer WA-1C has a sharp upper contact with overlying layer WA-1D, which varies in thickness from 2.5–19 cm and mostly is composed of fine ash with a few layers of lapilli. The WA-2 deposit lies on top of Cone 2 basaltic tephra with a sharp, noneroded contact. WA-2 lacks the obvious internal layering characteristic of WA-1, although the bottom and top of WA-2 are enriched in lapilli with gradational transitions to fine ash in the center of the section.

3b Granulometry

Grain-size distributions for the 1975 Tolbachik eruption lack systematic variations throughout the studied sections (Figure 4). Ten representative sections were sampled (Figure 2) using standard sieving methods. Sampled unit thicknesses were normalized to cumulative percent of total deposit thickness for the Cone 1 and Cones 2–3 eruptions, to compare equivalent stratigraphic intervals. The marked decrease in sorting and median diameter shown in the uppermost samples of three Cone 2–3 sections (Figure 4) is likely due to infiltration of fines from eolian processes and not from eruption processes. Although significant variations exist in median diameter and sorting within each eruption sequence (Figure 4), the absence of systematic variations within the deposit is surprising given the reported variations in tephra-column heights. The highest tephra columns (6–10 km) were reported early in the Cone 1 eruption. With relatively constant prevailing winds, larger particles should travel further downwind before settling out of an initially higher tephra plume (e.g., Woods and Bursik, 1991). Lower tephra columns (2–3 km) later in the Cone 1 eruption would be expected to result in finer median grain-sizes at a constant distance from the vent. Possible explanations for the absence of systematic grain-size variation include relatively lower wind speeds early in the Cone 1 eruption or insensitivity of proximal (i.e., 3–7 km) fall deposits to 4–7 km variations in column height.

The 1975 Tolbachik fall deposit was unusually dispersive and fragmented, relative to other basaltic fall deposits. Using the methods of Walker (1973) and not including WA-1 or WA-2 in the analysis, the 1975 Tolbachik fall deposit has an extrapolated maximum thickness of 3.5 m. Eruption dispersivity is measured by the area enclosed by an isopach with 1 percent of this thickness (Walker, 1973). Most strombolian fall deposits have a dispersivity of <10 km^2, however, dispersivity for the 1975 Tolbachik fall is at least 300 km^2. The 1975 Tolbachik falls also are highly fragmented, relative to other

strombolian falls. Detailed grain-size data for the complete Tolbachik fall deposit are only available for sections ≥0.30 m thick. Using analyses for section T33 (Figure 2) at the 0.30-m isopach, 47 percent of the Tolbachik fall deposit is finer than 1 mm. In contrast, strombolian fall deposits have <10 percent of the ash finer than 1 mm (Walker, 1973). This degree of fragmentation also is greater than commonly observed for subplinian eruptions of comparable dispersivity, but less than found for many hydrovolcanic eruptions (Walker, 1973). The 1975 Tolbachik eruption is best classified as a violent strombolian eruption, being more dispersive and fragmented than basaltic strombolian or subplinian eruptions.

Grain-size distributions for white-ash samples were determined using a MALVERN Laser Particle Sizer 3600E, which circulates the sample to ensure complete particle disaggregation. Size distributions were analyzed using the sequential fragmentation and transportation model of Sheridan et al. (1987) and Wohletz et al. (1989).

WA-1 deposits exhibit three main granulometric features that are distinct from Cones 1–3 basaltic fall deposits: (i) very poor sorting due to abundant fine ash, (ii) bimodal or multimodal grain-size distributions, and (iii) increase in the abundance of the finer fraction and depletion of the coarser fraction upward in the sections (Figures 3, 5). The coarser-grained mode in WA-1 overlaps the size distribution from the underlying Cone 1 fall deposit (Figure 5), although the mean diameter of the WA-1 coarser mode is generally 2–3 φ finer than the Cone 1 falls. The coarser mode in WA-1 also decreases in median diameter from around −1 φ to 2 φ between 1 and 4.4 km from the vent, whereas the median diameter for the underlying Cone 1 falls only decreases from −2.2 φ to −1.2 φ across that distance. WA-2 deposits also are characterized by poor sorting, abundant fine ash, and bimodal grain-size distributions (Figure 5). In contrast to WA-1 falls, WA-2 falls lack a prominent lapilli-sized mode and are characterized by coarse- and fine-ash modes (Figure 5).

Presence of bimodal or multimodal grain-size distributions in pyroclastic deposits is usually attributed to the simultaneous deposition of grains transported by different flow mechanisms (Sheridan et al., 1987; Wohletz et al., 1989). 1975 Tolbachik white-ash deposits are massive and have uniform thickness over topographic irregularities, consistent with a fall origin. The presence of multimodal grain-size distributions in the white-ash deposits indicates that multiple fragmentation processes occurred during the formation and transport of white-ash clasts. In contrast, basaltic strombolian fall deposits are characterized by a simple Gaussian grain-size distribution, reflecting a single mechanism for magma

fragmentation and pyroclast transport (e.g., Walker and Croasdale, 1972; Wohletz, 1983). Although few data are available for comparison, violent strombolian fall deposits such as 1975 Tolbachik (Figure 5) and 1943 Parícutin (e.g., Segerstrom, 1950) also have simple Gaussian grain-size distributions.

Tolbachik white-ash deposits have fragmentation and dispersivity characteristics quite similar to phreatomagmatic fall deposits (Walker, 1973). Although data are not available for deposits at 1 percent of the maximum deposit thickness, ≥90 percent of the WA-1 deposit is finer than 1 mm at site T14 (Figure 2). The interpreted area of the isopach enclosing 1 percent of the maximum WA-1 deposit thickness is 80–100 km^2, comparable to silicic phreatoplinian eruptions (e.g., Self and Sparks, 1978). The smaller-volume WA-2 is more comparable to surtseyan deposits (Walker, 1973), as WA-2 has a dispersivity of 30 km^2 and ≥95 percent of the deposit is finer than 1 mm at site T17 (Figure 2).

In spite of a high degree of fall-deposit fragmentation and dispersion, median diameter and sorting characteristics of the 1975 Tolbachik magmatic falls are typical for normal strombolian deposits (Figure 6). This suggests that the relatively large eruption columns and extensive dispersion of the 1975 Tolbachik eruption may be related more to large and sustained mass-flow rates than to a fundamental change in magma fragmentation behavior. Tolbachik white-ash deposits are more poorly sorted and finer grained than most magmatic falls (Figure 6) and plot in the range of phreatomagmatic deposits (Walker and Croasdale, 1972).

3c Morphology of Pyroclasts

Tephra clasts from the 1975 Tolbachik magmatic eruption have morphological features typical of basaltic strombolian eruptions (e.g., Heiken and Wohletz, 1985). Juvenile fall deposits are characterized by (i) achneliths of relatively low vesicularity with fluidal textures and smooth, glassy surfaces (Figure 7a), and (ii) more equant, highly vesicular sideromelane pyroclasts with smooth, glassy surfaces and partly crystalline groundmass (Figure 7b). Pyroclast surfaces for both morphological types are fresh and lack secondary mineralization. Achneliths constitute about 15 percent of the pyroclasts from early Cone 1 deposits, which corresponds to the most energetic phase of the eruption. Achnelith abundance increases to 40 percent in deposits formed near the end of the Cone 1 eruption, consistent with observed trends of decreasing column height and dispersivity through the Cone 1 eruption. Following WA-1 formation, achneliths constitute 40 percent of the Cone 2–3 fall deposit, which increases to 75 percent for the latest

stages of the Cones 2 and 3 eruption. These trends support the use of achnelith abundances as a qualitative measure of eruption dispersivity (i.e., Walker and Croasdale, 1972).

Juvenile pyroclasts in WA-1 and WA-2 deposits are morphologically distinct from other 1975 Tolbachik fall deposits and exhibit clear hydromagmatic fragmentation features. Achneliths are absent from the WA-1 and WA-2 deposits. Pyroclasts with convoluted, highly irregular surfaces (Figure 7c) dominate the juvenile component in WA-1 and WA-2. These surfaces likely form during turbulent mixing between water and magma when repeated vapor-film collapse forms high surface-area particles (Wohletz, 1983). Subordinate amounts of sideromelane pyroclasts also are present in the white-ash deposits (Figure 7d). Sideromelane pyroclasts have lower vesicularity and are more angular and blocky than sideromelane pyroclasts in the main 1975 fall deposits. These morphological features are consistent with formation by ductile fragmentation during a hydromagmatic episode. Both the moss-form (Wohletz, 1983) and sideromelane pyroclasts have secondary chlorides and sulfates of K, Fe, and Mg adhering to the clast surfaces. This vapor-phase mineralization must have occurred prior to deposition, as pyroclasts above and below WA-1 and WA-2 are not mineralized.

Accretionary lapilli and aggregated ash are common features of WA-1 and WA-2 deposits and further emphasize the role of hydromagmatic activity in white-ash formation. Accretionary lapilli (Figure 7e) form a loosely packed deposit with clasts ranging from 0.2–1 mm. Each lapillus consists of a core containing one to several larger clasts with a rim of aggregated fine-ash particles (Figure 7f). These accretionary lapilli thus resemble core-type lapilli of Schumacher and Schmincke (1991), which form at relatively higher moisture concentrations. Experiments by Schumacher and Schmincke (1995) showed that 15–25 weight percent binding fluid is necessary for the formation of core-type lapilli. Presence of accretionary lapilli in proximal deposits (<700 m from the vent) indicate formation was likely controlled by an initially high concentration of moisture in the tephra column rather than from atmospheric moisture incorporated by the propagating eruption plume.

3d Magmatic Water Contents

Magmatic water contents are important to understanding the characteristics of the 1975 Tolbachik eruption. Following the method of Hervig et al. (1989), we analyzed phenocryst glass inclusions and matrix-glass water contents using a Cameca IMS 3f ion microprobe. Glass inclusions in

1975 Tolbachik phenocrysts are small and scarce. Melt inclusions in olivine phenocrysts contain 2.4 weight percent water and augite phenocrysts contain 1.9 weight percent water. Reproducibility of these analyses was ±0.3 weight percent, yielding an average water content of 2.2±0.4 weight percent. Matrix glass analyses could not be distinguished from background measured on olivine phenocrysts (i.e., <0.3 weight percent). In contrast, magmatic water contents for the 1975 Tolbachik eruption have been estimated from 3 weight percent (Tokarev, 1978) up to 9 weight percent (Slezin and Fedotov, 1984).

3e Xenoliths

Xenoliths derived from the Quaternary Tolbachik mafic platform and Neogene Shapinskaya formation are distributed throughout the deposits of the 1975 Tolbachik eruption. Variations in xenolith abundance provide useful information on the nature of the subvolcanic conduit prior to and after white-ash events, and on subsurface processes associated with this violent strombolian eruption. Xenoliths from juvenile fall deposits were separated from the -3φ–0φ-size classes with a binocular microscope and weighed for each sampled stratigraphic interval. Light-colored xenoliths from the Shapinskaya formation and megaplagiophyric lavas were easily identified. Dark-colored Quaternary lavas, however, were difficult to distinguish from poorly vesiculated juvenile pyroclasts and thus may be underestimated in these fall deposits. Weight percentages were corrected to volume percentages using average densities of 2600 kg m^{-3} for sedimentary and volcanic xenoliths and 1700 kg m^{-3} for juvenile scoria. Xenolith abundances were normalized to account for the size-class abundances in the total sample, producing an average xenolith abundance for each sampled interval (Figure 8). Although no regular variations are apparent in xenolith abundance up-section, there is a tendency for higher xenolith abundances (>0.1 volume percent) to occur in the upper half of proximal Cone 1 sections (Figure 8). Xenolith abundances also appear highest in the base of the most proximal Cone 2–3 section. Normalizing each sampled interval to total deposit thickness gives average xenolith abundances of 0.03–0.3 percent for Cone 1 sections and 0.01–0.07 percent for Cone 2–3 sections (Figure 8).

Coarse lag deposits on cone flanks and lava flows can provide data on xenolith types and abundances at a higher resolution than possible in more distal tephra-fall deposits. These xenolith abundances were determined by measuring the size and number of xenoliths within 30–40 m^2 areas. Xenoliths on the outer southern flanks of Cone 1 preserve the latest stage activity at that vent and correspond to lag deposits from the WA-1 event. These xenoliths constitute 11 percent of the surface

deposit on Cone 1, with Shapinskaya formation rocks comprising 30 percent and Quaternary mafic rocks the remaining 70 percent of the xenoliths. Xenoliths on late-stage Cone 2 lavas are 1 percent and on the outer flanks of Cone 2 are 2 percent, respectively. Shapinskaya formation rocks, however, constitute 76 percent of these xenoliths.

An unusual type of xenolith-rich bomb occurs on the flanks of Cone 1, which preserves a rapid pulse of subsurface brecciation associated with the WA-1 event. These breccia bombs contain 30–40 volume percent xenoliths of the same types and thermal histories as those erupted individually. Included xenoliths reach 5 cm in diameter and are supported within a quenched, microvesicular basalt matrix (Figure 9). For any specific rock type of constant size, xenoliths range from fresh and angular without any thermal effects to partially melted and deformed. Small areas of some xenoliths are glassy, which indicates the areas melted and were quenched during ascent. The diverse pyrometamorphic effects indicate that rocks adjacent to and for some distance outward from the subvolcanic conduit were entrained by the same event. In contrast, xenolith-rich bombs from hydrovolcanic eruptions commonly lack pyrometamorphic effects (e.g., Fisher and Schmincke, 1984, p. 239). The mixture of rock types within the breccia bombs could only occur if these rock types were ascending simultaneously in the conduit when quenched. Rock types are distributed randomly with distance from the bomb margin, whereas zonation would be expected if the rock fragments accreted sequentially. The bombs are massive and not layered, which would likely occur if the bomb formation represented multiple fragmentation and entrainment events. Although individual xenoliths are common on the upper surfaces of Cone 1 lavas, which represent earlier stages of the eruption, breccia bombs were not found on the lavas after several dedicated searches. The unusual lithological characteristics and occurrence only on the flanks of Cone 1 indicates the breccia bombs correlate with the WA-1 event.

Up to 75 volume percent of the white-ash deposits consist of crustal xenoliths derived from the Quaternary mafic platform and Shapinskaya formation. Component analysis of the white ashes was conducted by counting a total of 2000 particles in the -1φ–3φ-size classes using a binocular microscope. Based on qualitative SEM observations, xenoliths constitute at least 80 volume percent of the 4φ–10φ-size classes. Xenoliths in WA-1 are dominated by mafic platform lavas (Figure 10a), as was observed in correlative xenolith aprons on Cone 1 (Figure 10b). Subequal amounts of Shapinskaya formation sedimentary and volcanic xenoliths also characterize WA-1 falls. In contrast, WA-2 xenoliths are dominated by Shapinskaya formation sedimentary rocks (Figure 10c, d). The amount of xenoliths also

increases upward in the WA-1 section (Figure 3b). Sedimentary xenoliths are more abundant in the upper part of the WA-1 deposit, indicating xenolith source regions became progressively deeper during the WA-1 event (Figure 3b).

4 DISCUSSION

During initial magma ascent, dikes propagate vertically through elastic strain of horizontally stressed wall-rock accompanied by minor wall-rock stoping (Delaney et al., 1986; Lister and Kerr, 1991). For observed basaltic cinder cone eruptions such as 1975 Tolbachik, a centralized vent is established within about a day of initial fissuring activity. Magma ascent localizes in a central conduit from the initial dike system, whereas magma stagnates in adjacent dikes lacking vertical flow (Delaney and Pollard, 1982; Bruce and Huppert, 1989, 1990). Erupted xenoliths thus are likely derived from wall rock close to the conduit and are not transported laterally in essentially stagnant dikes.

Xenolith abundances constrain the dimensions of the shallow subsurface conduit at several stages of the 1975 Tolbachik eruption. Subvolcanic conduit geometries are likely complex due to local variations in rock strength, fracturing, and strain partitioning (e.g., Spence and Turcotte, 1985; Delaney and Gartner, 1997). We assume for relative comparisons that the subvolcanic conduit is readily approximated by a vertical cylinder (e.g., Wilson et al., 1980). Tephra-fall deposits from Cone 1 (2.3×10^8 m^3) have average xenolith abundances of 0.13 volume percent. Assuming xenolith proportions are equivalent to WA-1, Cone 1 falls contain about 2.1×10^5 m^3 of Quaternary mafic platform xenoliths and about 0.9×10^5 m^3 of Shapinskaya formation xenoliths. If the initial magmatic conduit was 2 m in diameter (i.e., Bruce and Huppert, 1990) and the depth of the Quaternary-Shapinskaya contact is 1200±200 m, this volume of Cone 1 xenolith could be derived from a cylindrical annulus with a constant outer diameter of 15±2 m extending to 1.7±0.2 km depth (Figure 11). Varying the initial conduit diameter between 1 to 5 m produces a <5 percent change in these values. Cone 2 produced about 1.9×10^8 m^3 of tephra fall but has an average xenolith abundance of only 0.05 volume percent. Using WA-2 xenolith proportions, the calculated 3.4×10^4 m^3 of Quaternary mafic and 5.1×10^5 m^3 of Shapinskaya formation xenoliths in Cone 2 falls can be derived from a cylindrical annulus with an outer diameter of 6±1 m extending to 2.8±0.4 km depth.

Significant conduit widening occurred during the white-ash events. WA-1 has an *in situ* density of 1500 kg m^3. After removing a 30 percent juvenile component and correcting for an original rock density of 2600 kg m^3, 2.0×10^6 m^3 of Quaternary mafic platform and 0.8×10^6 m^3 of Shapinskaya formation rocks were ejected in the <12-hour WA-1 event. This volume corresponds to an annulus extending 1.7±0.3-km deep with an initial inner diameter of 15 m and an outer diameter of 48±4 m (Figure 11). The 1.6×10^4 m^3 of Quaternary mafic platform and 2.4×10^4 m^3 of Shapinskaya formation rocks contained in WA-2 can be derived similarly from an annulus extending 3.0±0.5-km deep with an initial inner diameter of 3 m and an outer diameter of 4±0.1 m.

The dynamics of two-phase flow (e.g., Vergniolle and Jaupart, 1986) can be used to interpret xenolith entrainment processes in Cones 1–3 magmatic tephra falls. Upward migration of earthquake epicenters between 27 June–6 July 1975 yields an initial magma ascent rate of 0.03–0.04 m s^{-1} (Fedotov et al., 1976, 1984). Using the MELTS model of Ghiorso (1994) and assuming a constant gas-to-melt ratio, the initial magma had a vapor saturation pressure of 500–600 bar (i.e., about 2 km depth). The relatively slow rate of magma ascent facilitated magmatic degassing at <2 km and resulted in an initial stage of Cone 1 activity characterized by fire-fountaining and low-energy strombolian eruptions. These eruption features are characteristic of bubbly and slug-flow regimes (Jaupart and Vergniolle, 1988). Low gas fractions and low mass-flow rates under these flow regimes restrict the amount of differential shear stress on conduit walls, limiting wall-rock entrainment into the ascending magma (Jaupart and Tait, 1990; Macedonio et al., 1994).

Within 3–5 days, the partially degassed magma was cleared from the conduit and sustained tephra columns at Cone 1 averaged 5–8 km high. Magma ascent rate likely increased through localization of flow into a conduit bounded by stagnating and cooling dikes (e.g., Bruce and Huppert, 1989). Limited shallow magmatic degassing occurred, with most of the exsolved 2.2±0.4 weight percent water going to efficient magma fragmentation. This phase of sustained activity is likely characterized by droplet to drop-annular flow (Wallis, 1969; Vergniolle and Jaupart, 1986). Using the models of Wilson et al. (1980) and Wilson and Head (1981), the magma was likely fragmented by 500 m below the surface. Although flow velocities were highest above the fragmentation depth, there was surprisingly little xenolith entrainment accompanying early to middle Cone 1 activity (Figure 8). Many xenoliths also were derived from the Shapinskaya formation, which is at least 500 m below the magma fragmentation depth. Wall-rock abrasion is an important mechanism for xenolith production in fragmented silicic magmas (e.g.,

Macedonio et al., 1994), but may not be significant for fragmented basaltic magmas. The Cone 1 xenolith data suggest that conduit pressures at 0.5–2 km were consistently greater than lithostatic, or that shear stresses were negligible on conduit walls, inhibiting the formation of xenoliths relative to later periods of activity.

Most of the xenoliths in Cone 1 fall deposits occurred during the latest stages of activity, when lavas also were erupting. Tephra-column heights also were lower during the latest stages of Cone 1 activity and accompanied by short interruptions in explosive activity. Eruptions at Cones 2–3 had the same characteristics as late Cone 1 activity. Simultaneous eruption of tephra columns and lava flows likely indicates an annular flow regime, in which partially degassed magma accretes to the conduit walls and is diverted laterally to form bocca-fed lavas (Vergniolle and Jaupart, 1986). Shear stress induced by upward flow of the gas-rich core supports the degassed annulus of magma. The interplay between removal of annular magma through lava formation and accretion of magma onto the annulus continues until the annulus reaches a critical thickness and collapses. This transient decrease in conduit pressure below lithostatic allows previously stressed wall-rock to collapse inward along with the annulus, effectively plugging upward flow in the conduit (Macedonio et al., 1994). Continued degassing and upflow of magma in the conduit increases the pressure on the plug until it fragments and the eruption continues. During the last week of Cone 1 activity, hiatuses in the tephra eruption increased from seconds to hours in duration. Lava continued to flow from boccas during these longer hiatuses, indicating that partially degassed magma was still ascending from the conduit system. The increasing duration of tephra hiatuses can be accounted for by progressive widening of the conduit through wall-rock removal. As the conduit widens, the net volume of the accreted annulus would increase if mass-flow rates in the central core remained relatively constant. Progressively larger volumes of annular collapse would require larger conduit pressures to break the plug and continue the eruption. By the end of Cone 1 juvenile activity, an outer annulus diameter of 15±2 m likely supported an accreted magma volume sufficient to terminate the eruption when the accreted magma collapsed and plugged the conduit.

Xenolith formation during the white-ash events involved significant interaction between magma, heated wall-rock, and meteoric water. Juvenile tephra in WA-1 and WA-2 falls show morphological features characteristic of hydromagmatic fragmentation (e.g., Wohletz, 1983), whereas juvenile tephra in other Cones 1–3 falls only preserve magmatic fragmentation effects. Pyroclast surfaces in the white-ash falls have ubiquitous secondary chloride and sulfate minerals, whereas magmatic falls lack this

mineralization. Core-type accretionary lapilli occur throughout the Tolbachik white-ash fall deposits, which need 15–25 weight percent fluid to form (Schumacher and Schmincke, 1995). Tolbachik white-ash deposits are characterized by up to 75 volume percent xenoliths, as are many hydrovolcanic falls (Self et al., 1980; Wohletz, 1986; Houghton and Nairn, 1991; Dzurisin et al., 1995). Most of the WA-1 and WA-2 falls consist of xenoliths pulverized to very fine ash, whereas xenoliths in juvenile falls are sparse and concentrated in the coarse-ash fraction. Phreatomagmatic falls typically show similar decreases in average grain-size relative to magmatic falls (e.g., Wohletz and Sheridan, 1983; Wohletz, 1986).

An unusual feature of the 1975 Tolbachik basaltic eruption is that the hydromagmatic events occurred relatively late in the eruption sequence. Basaltic hydromagmatic eruptions typically occur when ascending magma intersects abundant water at the surface or shallow subsurface; confining pressures above 2–3 MPa are sufficiently high to suppress explosive expansion of water to vapor (e.g., Lorenz, 1986). Deeper steam explosions can occur, however, if induced by localized reductions in rock strength (Wohletz, 1986) or by downward migration of the magma-water interaction zone (Lorenz, 1986). If a dry-out zone is eventually established around the conduit, the early hydromagmatic phase of the eruption typically grades into a wholly magmatic period at the end of the eruption (Crowe and Fisher, 1973; Wohletz and Sheridan, 1983; Wohletz, 1986; Houghton and Hackett, 1984; Houghton and Nairn, 1991). At Tolbachik, the 500-m depth to the water table (i.e., 10–13 MPa) was sufficient to suppress explosive expansion of water during initial stages of the eruption. Heat transfer from the conduit likely created a thermal pressurization gradient to groundwater flow, resulting in outflow of water from the conduit area (Parmentier and Schedl, 1981; Delaney, 1982). Wall-rock fracturing also accompanied the eruption in response to thermal expansion and, more importantly, overpressure created by flow in the conduit (Spence and Turcotte, 1985; Heiken et al., 1988). The disturbed zone around the conduit continued to develop throughout the Cone 1 eruption, along with conductive heating of wall rock following significant accretion of magma to the conduit walls.

On 7 August 1975, the 9 hour and 2–3 hour hiatuses in the Cone 1 eruption were sufficient to allow groundwater entry into the conduit area and initiate the WA-1 event. The mixture of pyrometamorphosed and fresh xenoliths in cone apron deposits and breccia bombs clearly indicates that wall-rocks adjacent to and outward from the conduit were mixed in the same instantaneous event. Several mechanisms likely contributed to this disruptive event. Stagnation of flow in the conduit would have reduced the effective pressure on conduit walls, allowing fractures to dilate in response to reduced

horizontal stress (Spence and Turcotte, 1985). This reduction in conduit pressure alone, however, does not appear sufficient to initiate the WA-1 event (e.g., Dobran and Papale, 1993), as there were 9-hour and 2–3-hour hiatuses in activity before the white-ash eruption. Conduit walls probably collapsed during this hiatus in activity, creating a pressure transient in the disturbed wall-rock zone sufficiently low to initiate explosive expansion of inflowing groundwater (i.e., Dvorak, 1992). The observed decrease in average grain-size and increase of xenolith abundance upward in the WA-1 section (Figure 3) can be explained by a progressive increase in the water-to-magma ratio, resulting in greater fragmentation efficiency (Wohletz, 1986). Magma diversion from the Cone 1 conduit northward to the site of Cone 2 allowed groundwater to quench the WA-1 eruption.

The WA-2 eruption occurred at Cone 2 on 16 August 1975, when a relatively large amount of magma was diverted northward from the main conduit to the site of Cone 3. Reduction in Cone 2 conduit pressure induced by the magma diversion likely allowed groundwater inflow into the disturbed zone around the >500-m-deep wall rocks (i.e., Dobran and Papale, 1993). This disturbed zone was small relative to Cone 1, due to the short duration of the Cone 2 eruption prior to groundwater inflow. For both the WA-1 and WA-2 events, the initiating process appears to be dramatic reductions in conduit pressure related to development of a new vent system, allowing >500-m-deep groundwater to invade the conduit area and expand explosively. Although magma-water interactions can occur in many large eruptions where the magma is highly fragmented (Dobran and Papale, 1993), the 1975 Tolbachik eruption shows that similar interactions can occur in small-volume basaltic systems below likely magma fragmentation depths.

Five basaltic volcanoes younger than about 1 Ma are located within 20 km of the proposed high-level radioactive waste repository site at Yucca Mountain, Nevada. The youngest of these volcanoes, 0.08 Ma Lathrop Wells (Heizler et al., 1997), has some features remarkably similar to deposits from the 1975 Tolbachik Cone 1 eruption. Similar features also occur at the 0.3 Ma Sleeping Butte volcanoes, but are less well developed than at Lathrop Wells volcano. Although early stages of the Lathrop Wells eruption were hydrovolcanic, with sparsely preserved dry-surge deposits extending outward to 1 km from the vent, the main cone-building stage of the eruption was dominantly magmatic (Wohletz, 1986). Lathrop Wells cone is constructed of fragmented tephra in reversely-graded beds formed by grain-flow of over-steepened fall deposits (i.e., Sohn and Chough, 1993). This process also was observed throughout the Cone 1 eruption (Fedotov et al., 1984). The hawaiite magma at Lathrop Wells (Vaniman et al., 1981)

has a similar crystallinity and calculated viscosity as the high-MgO 1975 Tolbachik basalts. Mineralogical relationships indicate the Lathrop Wells magma also contained approximately 2 weight percent water (i.e., Knutson and Green, 1975). Xenoliths are unusually abundant in the nonhydrovolcanic Lathrop Wells cone deposits and average about 1 volume percent for the <0.7 mm size fractions (Crowe et al., 1986, Wohletz 1986). Nearly all xenoliths were derived from a Tertiary ignimbrite section that is about 550 m thick beneath Lathrop Wells (Swadley and Carr, 1987). The abundance of Lathrop Wells xenoliths >1 mm in diameter was calculated from seventeen 1-m^2 cone sections using computer-assisted image analysis. After correcting for 15 percent deposit porosity, Lathrop Wells xenoliths >1 mm average 0.9 volume percent with a standard deviation of 0.6 volume percent. In comparison, basaltic spatter and cinder cones typically have xenolith abundances <0.06 volume percent (Valentine and Groves, 1996). The outer flanks of Lathrop Wells cone also contain distinctive breccia bombs that contain a mixture of fresh and pyrometamorphosed tuffaceous xenoliths (Figure 9b).

The xenolith abundances and breccia bombs at Lathrop Wells volcano indicate a white-ash event similar to 1975 Tolbachik likely occurred toward the end of this eruption. Most tephra-fall deposits have been eroded from Lathrop Wells volcano, however, analogy with Cone 1 can be used to estimate the volume of material potentially disrupted by Lathrop Wells. Basaltic cinder cone eruptions that sustained tephra columns have cone-to-fall ratios from around 1 (e.g., 1973 Heimaey, Self et al., 1974) to >6 (e.g., 1943 Parícutin, Segerstrom, 1950), with 2.5 for Tolbachik Cone 1. If Lathrop Wells falls were proportionally similar to Cone 1 and contained similar xenolith abundances, the conduit diameters were around 8 m toward the end of the Lathrop Wells eruption. Eruption duration and mass-flow rate control the extent of wall-rock disturbance around the conduit. Lathrop Wells has an estimated dense-rock volume of 8×10^7 km^3, which is about one-third the volume of Cone 1. Scaling the WA-1 deposit by one-third gives an estimated volume of around 10^6 m^3 disrupted by the Lathrop Wells white-ash event, which corresponds to an increase in conduit diameter to around 50 m.

The water table currently is located 700–600 m below ground surface at the proposed Yucca Mountain repository site (e.g., Luckey et al., 1996). In the unlikely event a basaltic volcano formed at the proposed site, this depth to the water table would suppress initial hydromagmatic activity unless initiated by unanticipated reductions in confining pressure (Crowe et al., 1986). Interpretations of eruptive style from sparsely preserved deposits around Yucca Mountain are currently subjective, but indicate that violent strombolian eruptions may characterize roughly half of the Quaternary basaltic volcanoes in the

Yucca Mountain system. Reductions in conduit pressure associated with bocca formation or waning stages of a future Yucca Mountain eruption may trigger hydromagmatic white-ash events, which enlarge subsurface conduits on the order of 50 m in diameter. This degree of conduit enlargement may potentially entrain and disperse more high-level radioactive waste that would be accounted for by strictly magmatic activity, and should be included in models that evaluate long-term performance of the proposed Yucca Mountain repository.

5 ACKNOWLEDGMENTS

Discussions with Markus Bursik, Mike Sheridan, and Chuck Connor helped to clarify and focus many aspects of this work. Yuri Doubik, Alexander Ovsyannikov, Yuri Taran, Vyacheslav Shapar, and Mike Conway provided expert assistance in Kamchatka and personal information on the Tolbachik volcanoes and their deposits. Detailed technical reviews by Chuck Connor significantly improved the quality of this manuscript. Technical assistance from Barbara Long, Annette Mandjuano, Lena Krutikov, and Ron Martin is gratefully acknowledged. The work reported here was supported by the U.S. Nuclear Regulatory Commission (Contract NRC-02-97-009). This work is an independent product of the CNWRA and does not necessarily reflect the views or regulatory position of the NRC.

6 REFERENCES

Balesta, S.T., Kargapol'tsev, A.A., and Grigoryan, G.B., 1983. The structure of the new Tolbachik volcanoes from seismic data. In: S.A. Fedotov and Ye.K. Markhinin (Editors), The Great Tolbachik Fissure Eruption. Cambridge University Press, New York, NY, pp. 316–326.

Balesta, S.T., Zubin, M.M., Kargopoltsev, A.A., and Fedorchenko, I.A., 1984. Deep structure of eruption region. In: S.A. Fedotov (Editor), Large Tolbachik Fissure Eruption, Kamchatka 1975–1976. Nauka, Moscow, Russia, pp. 514–536 (in Russian).

Braytseva, O.A., Melekestev, I.V., and Ponomareva, V.V., 1983. Age divisions of the Holocene volcanic formations of the Tolbachik Valley. In: S.A. Fedotov and Ye.K. Markhinin (Editors), The Great Tolbachik Fissure Eruption. Cambridge University Press, New York, NY, pp. 83–95.

Bruce, P.M., and Huppert, H.E., 1989. Thermal control of basaltic fissure eruptions. Nature, 342: 665–667.

Bruce, P.M., and Huppert, H.E., 1990. Solidification and melting along dykes by the laminar flow of basaltic magma. In: M.P. Ryan (Editor), Magma Transport and Storage. John Wiley & Sons, Chichester, England, pp. 87–101.

Budnikov, V.A., Markhinin, Ye.K., and Ovsyannikov, A.A., 1983. The quantity, distribution and petrochemical features of pyroclastics of the great Tolbachik fissure eruption. In: S.A. Fedotov and Ye.K. Markhinin (Editors), The Great Tolbachik Fissure Eruption. Cambridge University Press, New York, NY, pp. 41–56.

Connor, C.B., and Hill, B.E., 1995. Three nonhomogeneous Poisson models for the probability of basaltic volcanism: Application to the Yucca Mountain region, Nevada, U.S.A. Journal of Geophysical Research, 100: 10107–10125.

Connor, C.B., Lichtner, P.C., Conway, F.M., Hill, B.E., Ovsyannikov, A.A., Federchenko, I., Doubik, Yu., Shapar, V.N., and Taran, Yu.A., 1997. Cooling of an igneous dike 20 yr after intrusion. Geology, 25: 711–714.

Connor, C.B., Stamatakos, J., Ferrill, D., Hill, B.E., Magsino, S.B.L., LaFemina, P., and Martin, R.H., 1996. Integrating structural models into probabilistic volcanic hazard analyses: An example from Yucca Mountain, NV. EOS, Transactions of the American Geophysical Union, 77(46): F21.

Crowe, B.M., and Fisher, R.V., 1973. Sedimentary structures in base-surge deposits with special reference to cross-bedding, Ubehebe Craters, Death Valley, California. Geological Society of America Bulletin, 84: 663–682.

Crowe, B.M., Wohletz, K.H., Vaniman, D.T., Gladney, E., and Bower, N., 1986. Status of Volcanic Hazard Studies for the Nevada Nuclear Waste Storage Investigations, Los Alamos National Laboratory Report LA–9325–MS Vol. II, Los Alamos National Laboratory, Los Alamos, NM.

Delaney P.Y., 1982. Rapid intrusion of magma into wet rock: Groundwater flow due to pore pressure increases. Journal of Geophysical Research, 87: 7739–7756.

Delaney, P.T., and Gartner, A.E., 1997. Physical processes of shallow mafic dike emplacement near the San Rafael Swell, Utah. Geological Society of America Bulletin, 109: 1177–1192.

Delaney P.Y., and Pollard, D.D., 1982. Solidification of basaltic magma during flow in a dike. American Journal of Science, 282: 856–885.

Delaney, P.T., Pollard, D.D., Ziony, J.I., and McKee, E.H., 1986. Field relations between dikes and joints: Emplacement processes and paleostress analysis. Journal of Geophysical Research, 91: 4920–4938.

Dobran, F., and Papale, P., 1993. Magma-water interaction in closed systems and application to lava tunnels and volcanic conduits. Journal of Geophysical Research, 98: 14041–14058.

Doubik, Yu., Ovsyannikov, A.A., Connor, C., Martin, R., and Doubik, P., 1995. Development of the 1975 Tolbachik cinder cone alignment — nature of areal and lateral basaltic volcanism. EOS, Transactions of the American Geophysical Union, 76: F540.

Dvorak, J.J., 1992. Mechanism of explosive eruptions of Kilauea Volcano, Hawaii. Bulletin of Volcanology, 54: 638–645.

Dzurisin D., Lockwood, J.P., Casadevall, T.J., and Rubin, M., 1995. The Uwekahuna Ash Memeber of the Puna Basalt: Product of violent phreatomagmatic eruptions at Kilauea volcano, Hawaii, between 2800 and 2100 ^{14}C years ago. Journal of Volcanology and Geothermal Research, 66: 163–184.

Erlich, E.N., 1973. Modern structure and Quaternary volcanism of western part of Pacific ring. Nauka, Novosibirsk, Russia (in Russian).

Faberov, A.I. 1983. Activity of the Ploskiy Tolbachik volcano, June–July 1975. In: S.A. Fedotov and Ye.K. Markhinin (Editors), The Great Tolbachik Fissure Eruption. Cambridge University Press, New York, NY, pp. 36–40.

Fedotov, S.A., 1983. Chronology and features of the southern breakout of the Great Tolbachik fissure eruption, 1975–1976. In: S.A. Fedotov and Ye.K. Markhinin (Editors), The Great Tolbachik Fissure Eruption. Cambridge University Press, New York, NY, pp. 11–26.

Fedotov, S.A., Gorel'chik, V.I., and Stepanov, V.V., 1976. Seismological data on magma chambers, mechanisms, and evolution of the 1975 Tolbachik basalt fissure eruption on Kamchatka. Translations of the Transactions, Russian Academy of Sciences, 228(6): 1407–1410.

Fedotov, S.A., Chirkov, A.M., and Razina, A.A., 1984. Northern Breakout. In: S.A. Fedotov (Editor), Large Tolbachik Fissure Eruption, Kamchatka 1975–1976. Nauka, Moscow, Russia, pp. 11–74 (in Russian).

Fedotov, S.A., Balesta, S.T., Dvigalo, V.N., Razina, A.A., Flerov, G.B., and Chirkov, A.M., 1991. New Tolbachik Volcanoes. In: S.A. Fedotov and Yu. P. Masurenkow (Editors), Active Volcanoes of Kamchatka. Nauka, Moscow, Russia, p. 214–279 (in Russian).

Fierstein, J., and Nathenson, M., 1992. Another look at the calculation of fallout tephra volumes. Bulletin of Volcanology, 54: 156–167.

Fisher, R.V., and Schmincke, H.-U., 1984. Pyroclastic Rocks. Springer-Verlag, New York, NY, pp. 238–239.

Geist, E.L., Vallier, T.L., and Scholl, D.W., 1994. Origin, transport, and emplacement of an exotic island-arc terrane exposed in eastern Kamchatka, Russia. Geological Society of America Bulletin, 106: 1182–1194.

Ghiorso, M.S., 1994. Algorithms for the estimation of phase stability in heterogeneous thermodynamic systems. Geochimica et Cosmochimica Acta, 58: 5489–5501.

Heiken, G. and Wohletz, K., 1985. Volcanic Ash. University of California Press, Berkeley, CA.

Heiken, G., Wohletz, K., and Eichelberger, J., 1988. Fracture fillings and intrusive pyroclasts, Inyo Domes, California. Journal of Geophysical Research, 93: 4335–4350.

Heizler, M.T., McIntosh, W.C., Wilch, T.I., and Stroud, J., 1997. $^{40}Ar/^{39}Ar$ dating of basalts younger than 100 ka. EOS, Transactions of the American Geophysical Union, 78: F771.

Hervig, R.L., Dunbar, N., Westrich H.R., and Kyle, P.R., 1989. Pre-eruptive water content of rhyolitic magmas as determined by ion microprobe analyses of melt inclusions in phenocrysts. Journal of Volcanology and Geothermal Research, 36: 293–302.

Hill, B.E., Connor, C.B., Jarzemba, M.S., La Femina, P.C., Navarro, M., and Strauch, W., 1998. 1995 eruptions of Cerro Negro volcano, Nicaragua, and risk assessment for future eruptions. Geological Society of America Bulletin, 10: in press.

Houghton, B.F., and Hackett, W.R., 1984. Strombolian and phreatomagmatic deposits of Ohakune craters, Ruapehu, New Zealand: A complex interaction between external water and rising basaltic magma. Journal of Volcanology and Geothermal Research, 21: 207–231.

Houghton, B.F., and Nairn, I.A., 1991. The 1976–1982 Strombolian and phreatomagmatic eruptions of White Island, New Zeland: Eruptive and depositional mechanisms at a "wet" volcano. Bulletin of Volcanology, 54: 25–49.

Jarzemba, M.S., 1997. Stochastic radionuclide distributions after a basaltic eruption for performance assessments of Yucca Mountain. Nuclear Technology, 118(2): 132–141.

Jaupart, C., and Tait, S., 1990. Dynamics of eruptive phenomena. In: J. Nicholls and J.K. Russell (Editors), Modern Methods of Igneous Petrology: Understanding Magmatic Processes, Reviews in Mineralogy Vol. 24. Mineralogical Society of America, Washington, DC, pp. 211–238.

Jaupart, C., and Vergniolle, S., 1988. Laboratory models of Hawaiian and Strombolian eruptions. Nature, 331: 58–60.

Jayaweera, K.O.L.F., Seifert, R., and Wendler, G., 1976. Satellite observations of the eruption of Tolbachik volcano. EOS, Transactions of the American Geophysical Union, 57: 196–200.

Khramov, N.A. and Salin, U.S., 1966. Some questions of Eastern Kamchatka stratigraphy. In: Stratigraphy of the volcanogenic formations of Kamchatka. Nauka, Moscow, Russia, pp. 1–47 (in Russian).

Knutson, J., and Green, T.H., 1975. Experimental duplication of a high-pressure megacryst/cumulate assemblage in a near-saturated Hawaiite. Contributions to Mineralogy and Petrology, 52: 121–132.

Lange, R.A. 1994. The effect of H_2O, CO_2 and F on the density and viscosity of silicate melts. In: M.R. Carroll and J.R. Holloway (Editors), Reviews in Mineralogy, Volume 30: Volatiles in Magmas. Mineralogical Society of America, Washington, DC, pp. 331–369.

Lange, R.A., and Carmichael, I.S.E., 1987. Densities of Na_2O-K_2O-CaO-MgO-FeO-Fe_2O_3-Al_2O_3-TiO_2-SiO_2 liquids: New measurements and derived partial molar properties. Geochimica et Cosmochimica Acta, 51: 2931–2946.

Lister, J.R., and Kerr R.C., 1991. Fluid-mechanical models of crack propagation and their application to magma transport in dykes. Journal of Geophysical Research, 96: 10049–10077.

Lorenz, V., 1986. On the growth of maars and diatremes and its relevance to the formation of tuff rings. Bulletin of Volcanology, 48: 265–274.

Luckey, R.R., Tucci, P., Faunt, C.C., Ervin, E.M., Seinkampf, W.C., D'Agnese, F.A., and Patterson, G.L., 1996. Status of understanding of the saturated-zone ground-water flow system at Yucca Mountain, Nevada, as of 1995. Water-Resources Investigations Report 96-4077. U.S. Geological Survey, Denver, CO.

Maleyev, Ye.F., and Vande-Kirkov, Yu.V., 1983. Features of pyroclastics of the northern breakthrough of the Great Tolbachik Fissure Eruption and the origin of its pale-grey ash. In: S.A. Fedotov and Ye.K. Markhinin (Editors), The Great Tolbachik Fissure Eruption. Cambridge University Press, New York, NY, pp. 57–71.

Macedonio, G., Dobran, F., and Neri, A., 1994. Erosion processes in volcanic conduits and application to the A.D. 79 eruption of Vesuvius. Earth and Planetary Science Letters, 121: 137–152.

Melekestzev, I.V., Kraevaya, T.S., and Braitseva, O.A., 1970. Relief and deposits of young volcanic regions of Kamchatka. Nauka, Moscow, Russia (in Russian).

Parmentier, E.M., and Schedl A., 1981. Thermal aureoles of igneous intrusions: Some possible indications of hydrothermal convective cooling. Journal of Geology, 89: 1–22.

Schumacher, R., and Schmincke, H.-U., 1991. Internal structure and occurrence of accretionary lapilli – a case study at Laacher See Volcano. Bulletin of Volcanology, 53: 612–634.

Schumacher, R., and Schmincke, H.-U., 1995. Models for the origin of accretionary lapilli. Bulletin of Volcanology, 56: 626–639.

Segerstrom, K., 1950. Erosion Studies at Parícutin, State of Michoacán, Mexico. U.S. Geological Survey Bulletin 965–A. U.S. Geological Survey, Reston, VA.

Self, S., and Sparks, R.S.J., 1978. Characteristics of widespread pyroclastic deposits formed by interaction of silicic magma and water. Bulletin Volcanologique, 41: 196–212.

Self, S., Sparks, R.S.J., Booth, B., and Walker, G.P.L., 1974. The 1973 Heimaey strombolian scoria deposit, Iceland. Geological Magazine, 111: 539–548.

Self, S., Keinle, J., and Huot, J.-P., 1980. Ukinrek maars, Alaska, II. Deposits and formation of the 1977 craters. Journal of Volcanology and Geothermal Research, 7: 39–65.

Shanster, A.Ye., 1983. Basement xenoliths in the eruption products of the New Tolbachik Volcanoes and the problem of the formation of magma conduits in the upper crust. In: S.A. Fedotov and Ye.K. Markhinin (Editors), The Great Tolbachik Fissure Eruption. Cambridge University Press, New York, NY, pp. 72–82.

Shanzer, A.E., 1979. Structure of the framing of southern part of Klyuchevskaya group of volcanoes and features of tectonics and magmatism of Kronotsky-Tigil transverse zone. Bulletin of Volcanologic Stations, 56: 21–43 (in Russian).

Sheridan, M.F., Wohletz K.H., and Dehn, J., 1987. Discrimination of grain-size subpopulations in pyroclastic deposits. Geology, 15: 367–370.

Slezin, Yu. B., and Fedotov, S.A., 1984. Physical features of the eruption. In: S.A. Fedotov (Editor), Large Tolbachik Fissure Eruption, Kamchatka 1975–1976. Nauka, Moscow, Russia, pp. 143–176 (in Russian).

Sohn, Y.K., and Chough, S.K., 1993. The Udo tuff cone, Cheju Island, South Korea: Transformation of pyroclastic fall into debris fall and grain flow on a steep volcanic cone slope. Sedimentology, 40: 769–786.

Spence, D.A., and Turcotte, D.L., 1985. Magma-driven propagation of cracks. Journal of Geophysical Research, 90: 575–580.

Swadley, W.C, and Carr, W.J., 1987. Geologic Map of the Quaternary and Tertiary Deposits of the Big Dune Quadrangle, Nye County, Nevada, and Inyo County, California. U.S. Geological Survey Miscellaneous Investigations Series Map I–1767. U.S. Geological Survey, Reston, VA.

Tokarev, P.I., 1978. Prediction and characteristics of the 1975 eruption of Tolbachik volcano, Kamchatka. Bulletin Volcanologique, 41(3): 251–258.

Tokarev, P.I., 1983. Calculation of the magma discharge, growth in the height of the cone and dimensions of the feeder channel of Crater 1 in the Great Tolbachik Fissure Eruption, July 1975.

In: S.A. Fedotov and Ye.K. Markhinin (Editors), The Great Tolbachik Fissure Eruption. Cambridge University Press, New York, NY, pp. 27–35.

Valentine, G.A., and Groves, K.R., 1996. Entrainment of country rock during basaltic eruptions of the Lucero Volcanic Field, New Mexico. Journal of Geology, 104: 71–90.

Vaniman, D.T., Crowe, B.M., and Gladney, E.S., 1982. Petrology and geochemistry of Hawaiite lavas from Crater Flat, Nevada. Contributions to Mineralogy and Petrology, 80: 341–357.

Vergniolle, S., and Jaupart, C., 1986. Separated two-phase flow and basaltic eruptions. Journal of Geophysical Research, 91: 12842–12860.

Volynets, O.N., Flerov, G.B., Andreyev, V.N., Popolitov, E.I., Abramov, V.A., Petrov, L.L., Shcheka, S.A., and Selivanova, G.I., 1983. Geochemical features of the rocks of the Great Tolbachik Fissure Eruption 1975–1976 in relation to petrogenesis. In: S.A. Fedotov and Ye.K. Markhinin (Editors), The Great Tolbachik Fissure Eruption. Cambridge University Press, New York, NY, pp. 116–140.

Walker, G.P.L., 1973. Explosive volcanic eruptions – a new classification scheme. Geologische Rundsche, 62: 431–446.

Walker, G.P.L., and Croasdale, R., 1972. Characteristics of some basaltic pyroclastics. Bulletin of Volcanology, 35: 303–317.

Wallis G.B., 1969. One-Dimensional Two-Phase Flow. McGraw-Hill Book Company, New York, NY.

Wilson, L., and Head, J.W., III, 1981. Ascent and eruption of basaltic magma on the Earth and Moon. Journal of Geophysical Research, 86: 2971–3001.

Wilson, L., Sparks, R.S.J., and Walker, G.P.L., 1980. Explosive volcanic eruptions – IV. The control of magma properties and conduit geometry on eruption column behavior. Geophysical Journal of the Royal Astronomical Society, 63: 117–148.

Wohletz, K.H., 1983. Mechanisms of hydrovolcanic pyroclast formation: grain-size, scanning electron microscopy, and experimental studies. Journal of Volcanology and Geothermal Research, 17: 31–63.

Wohletz, K.H., 1986. Explosive magma-water interactions: Thermodynamics, explosion mechanisms, and field studies. Bulletin of Volcanology, 48: 245–264.

Wohletz, K.H., and Sheridan, M.F., 1983. Hydrovolcanic explosions II. Evolution of basaltic tuff rings and tuff cones. American Jounal of Science, 283: 385–413.

Wohletz K.H., Sheridan, M.F., and Brown, W.K., 1989. Particle size distributions and the sequential fragmentation/transport theory applied to volcanic ash. Journal of Geophysical Research, 94: 15703–15721.

Woods, A.W., and Bursik, M.I., 1991. Particle fallout, thermal disequilibrium and volcanic plumes. Bulletin of Volcanology, 53: 559–570.

FIGURE CAPTIONS

Figure 1. Location map for the 1975 Tolbachik eruption, constructed from 3-arc-second digital terrane elevation model. Contour interval 50 m. Tephra-fall isopachs for 1975 eruption in centimeters, from Budnikov et al. (1983), with tephra sample locations marked by "X". Gray shading is extent of lavas and cones from 1975–1976 activity. Triangles are locations of Quaternary basaltic vents, interpreted from field observations, SPOT imagery, and Fedotov et al. (1991). Inset map shows locations of major Quaternary volcanoes (circles). Italicized abbreviations: *PT* Plosky Tolbachik, *OT* Ostry Tolbachik, *1941* site of 1941 A.D. eruption, *1* Cone 1, *2* Cone 2, *3* Cone 3, *SC* Southern Cone. Universal Transverse Mercator, Zone 57, WGS-84 spheroid.

Figure 2. Location map for white-ash deposits from the 1975 Tolbachik eruption. Topographic base from Figure 1. Isopachs in centimeters for WA-1 (solid line) and WA-2 (dashed line). Sample locations marked by "X" with sample number in italicized text. Gray shading is interpreted extent of Cone 1 lavas and cone at time of WA-1 eruption, triangles are locations of Quaternary basaltic vents. Universal Transverse Mercator, Zone 57, WGS-84 spheroid.

Figure 3. (A) Photograph of WA-1 section T-24, showing major stratigraphic units. (B) Grain-size distributions and component analysis for WA-1 section T-24. Note decrease in average grain-size and increase in xenolith abundance and proportion of Shapinskaya formation upward in the section.

Figure 4. Median diameter and Inman sorting for 1975 Tolbachik fall deposits, sample locations in Figure 2.

Figure 5. Grain-size distributions for representative WA-1 and WA-2 fall deposits (A) WA-2 section T-17, (B) WA-2 section T-18, compared with WA-2 in section T-17, (C) WA-1 section T-22, and (D) WA-1 in section T-14. Sample locations on Figure 2.

Figure 6. Variations in median diameter versus sorting for magmatic 1975 Tolbachik falls are within limits expected for normal strombolian fall deposits (Walker and Croasdale, 1972). In contrast, white-ash falls have the fine grain-size and poor sorting characteristics of hydromagmatic falls.

Figure 7. Scanning electron microscope images of representative pyroclasts from 1975 Tolbachik fall deposits. (A) smooth-surface achnelith from magmatic fall, (B) vesicular sideromaline pyroclast from magmatic fall, (C) convoluted-surface pyroclast from hydromagmatic fall WA-1, (D) low vesicularity, blocky pyroclast from hydromagmatic fall WA-1. (E) Intact sample of WA-1, layer D, showing accretionary lapilli, and (F) enlarged view of lapilli surfaces in this sample.

Figure 8. Variations in total xenolith abundance for 1975 Tolbachik magmatic fall deposits. Xenolith abundances are in volume percent and sampled intervals are weighted to total section thickness, allowing comparison between different section locations. Sample locations on Figure 2.

Figure 9. Xenolith breccia bombs from 1975 Tolbachik Cone 1 and Lathrop Wells volcano, Nevada. Note mixture of different xenolith lithologies and variations in degree of pyrometamorphism on xenoliths.

Figure 10. Comparison of xenolith proportions between WA-1 and correlative lag deposits on Cone 1, and between WA-2 and correlative lag deposits on Cone 2 and adjacent lava flows.

Figure 11. Cross-section showing scale of subsurface conduit enlargement at Cone 1, relative to other geologic features. Note 2x horizontal exaggeration. Inverted triangle marks depth to water table. Although dimensions of upper breccia zone in crater are speculative, widening of the conduit to 48±4 m does not appear unwarranted for a cinder cone of these dimensions.

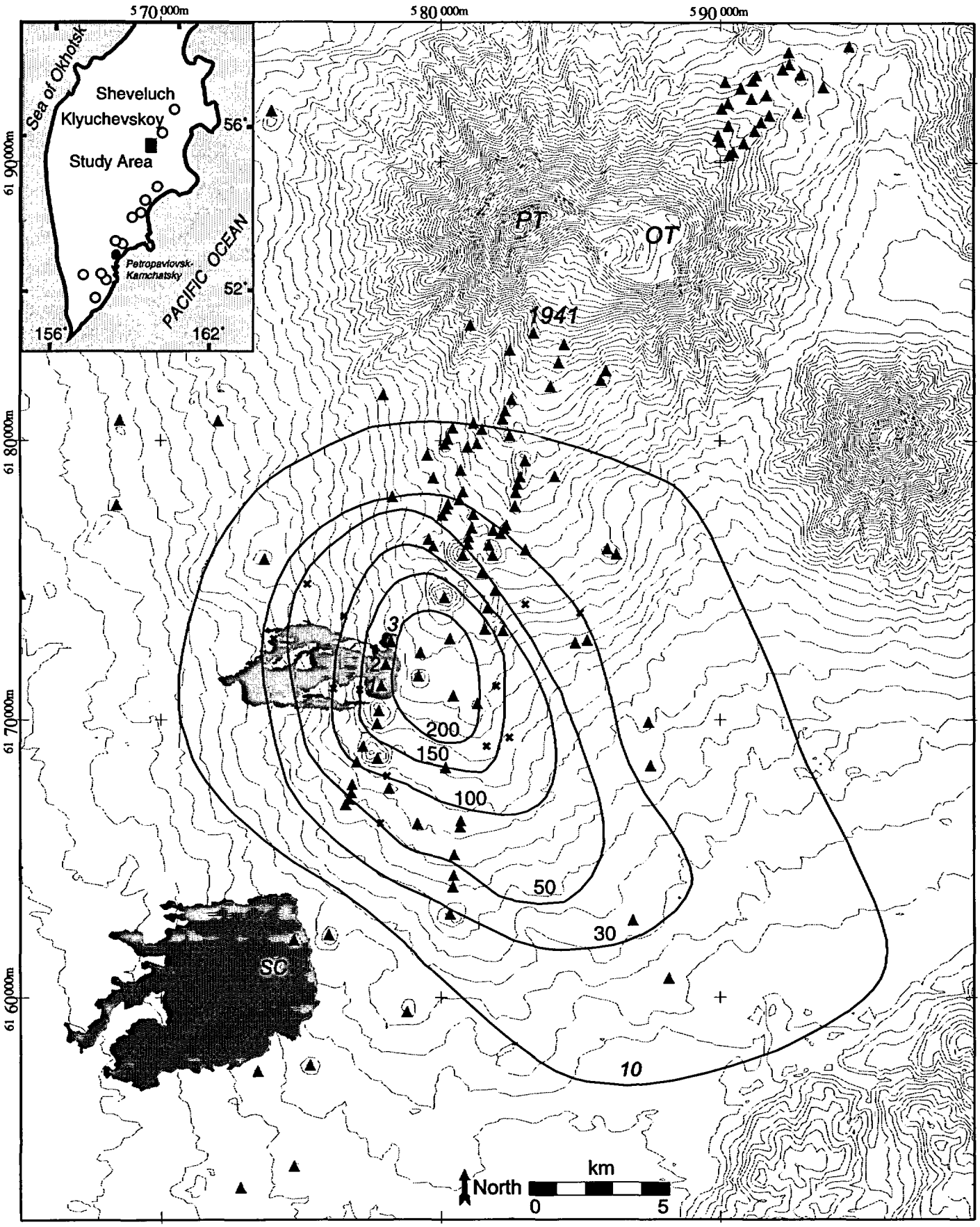

Doubik and Hill, Fig. 1

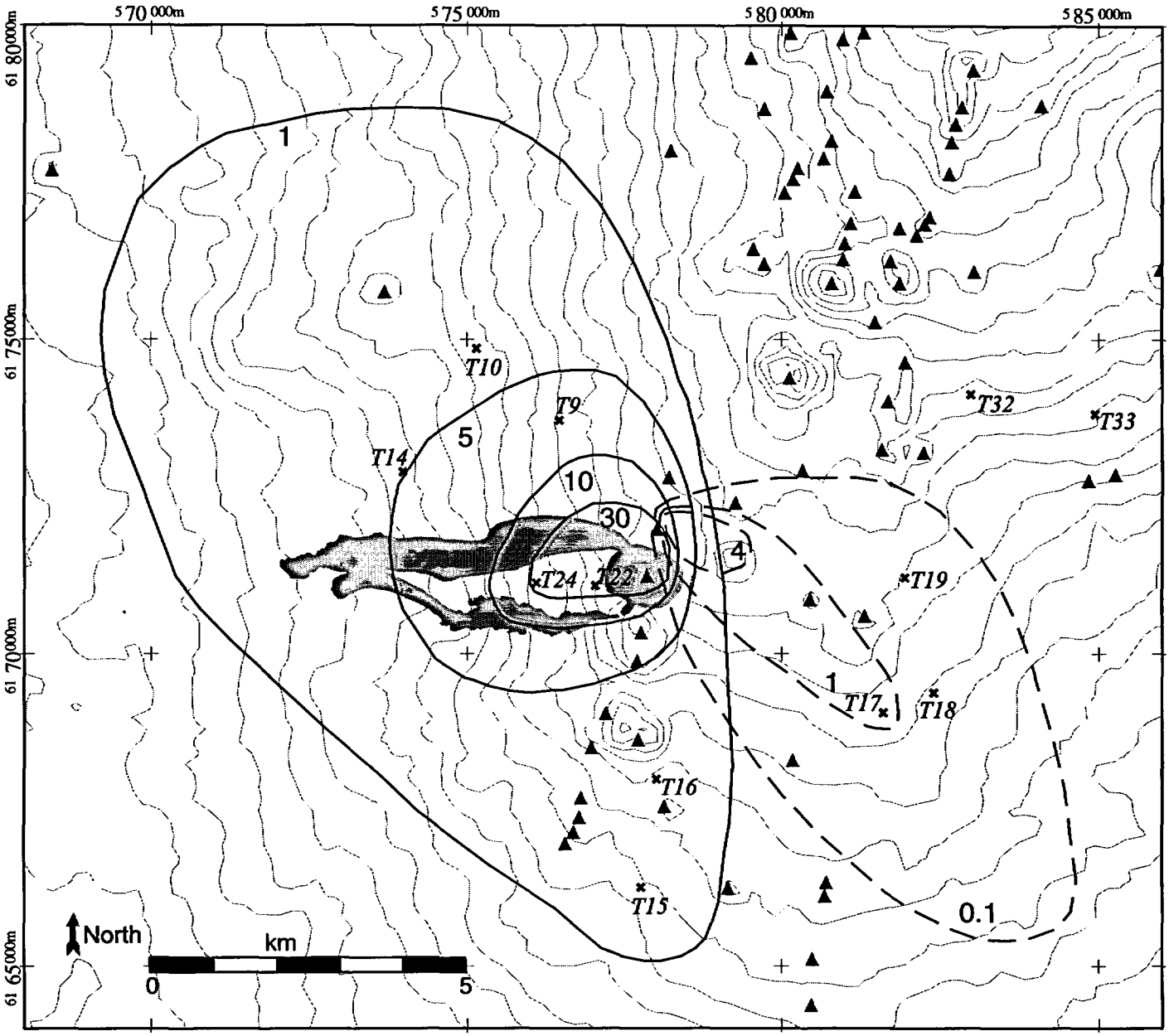

Doubik and Hill, Fig. 2

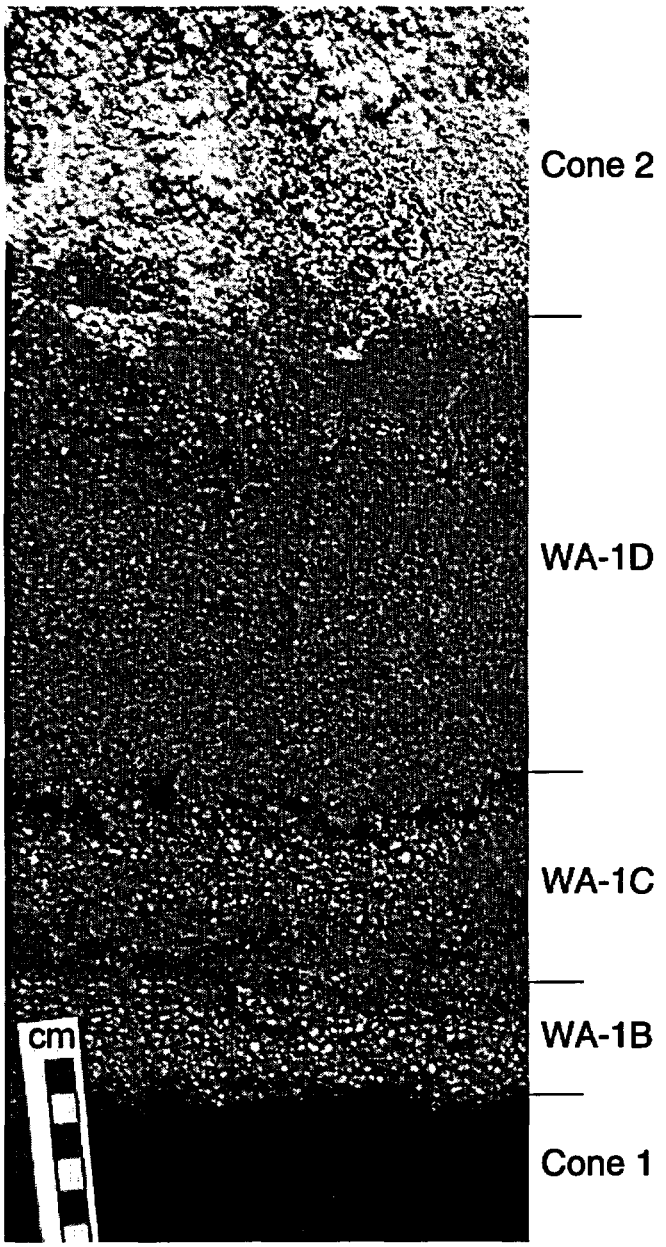

Section T-24

(A)

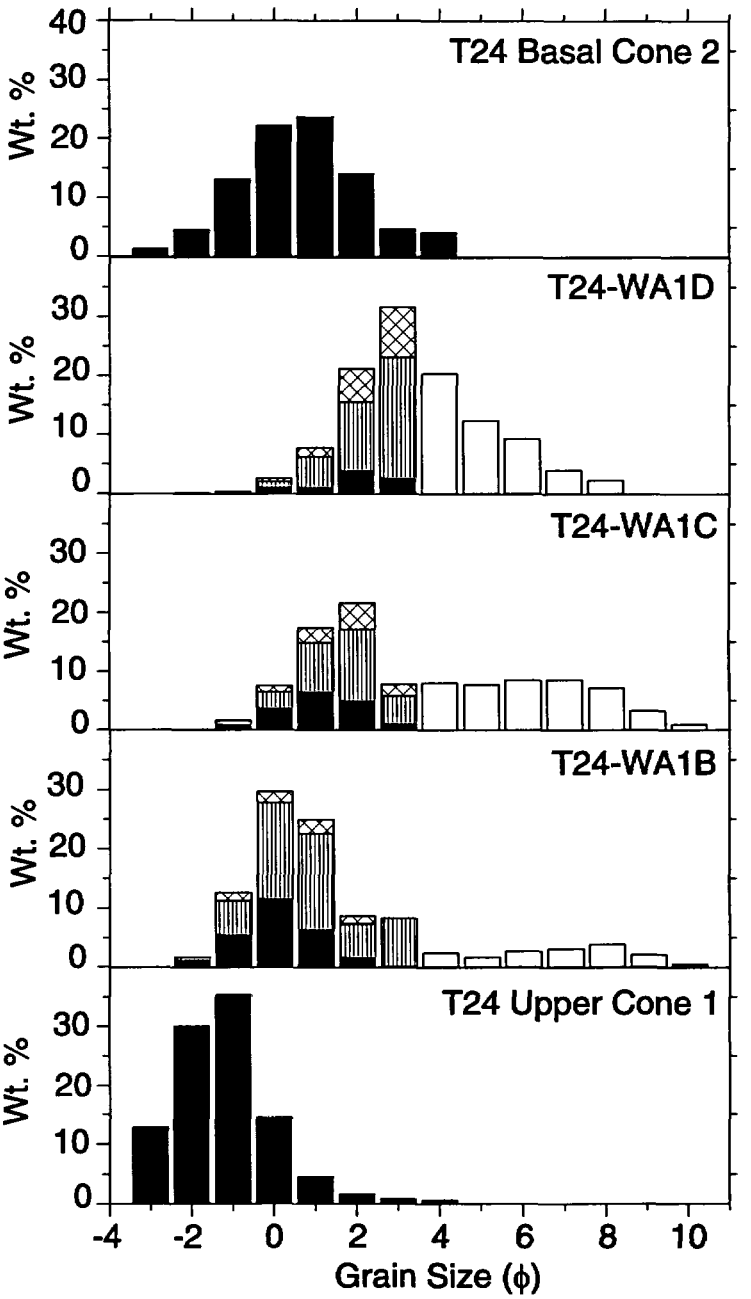

(B)

- Juvenile tephra
- Quaternary mafic platform rocks
- Shapinskaya Fm. sedimentary rocks
- Not separated

Doubik and Hill, Fig. 3

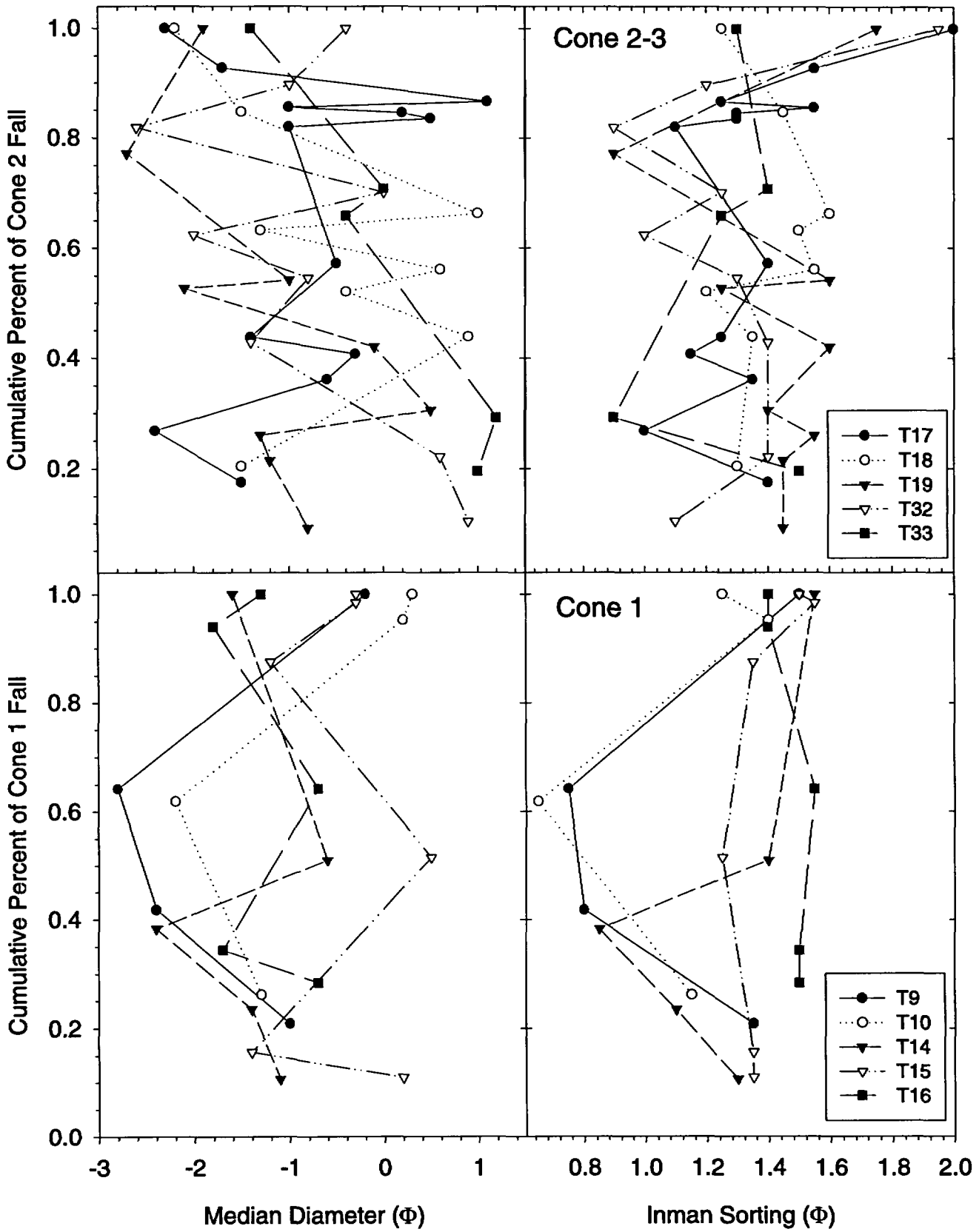

Doubik and Hill, Fig. 4

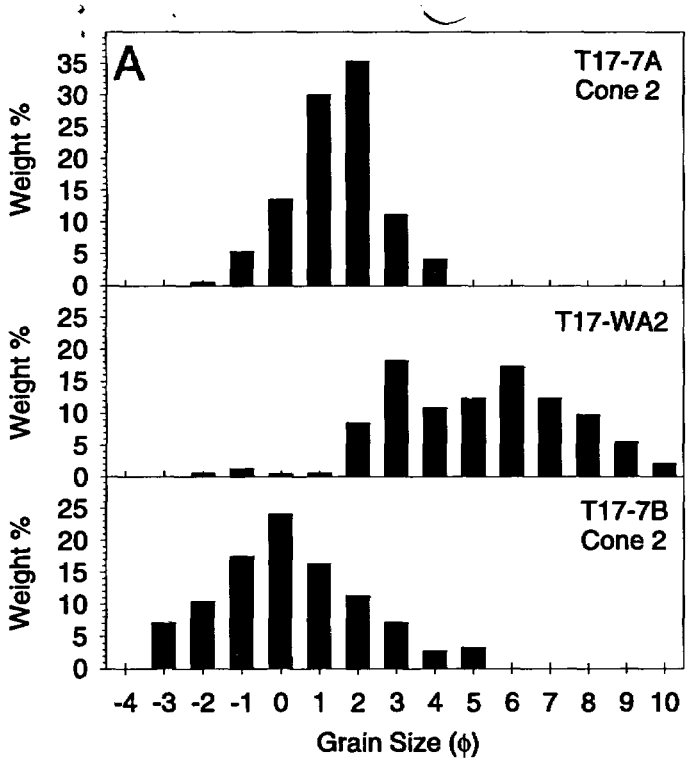

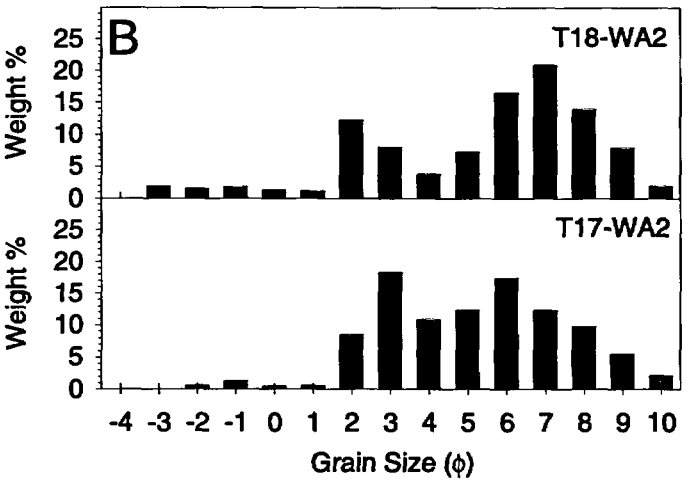

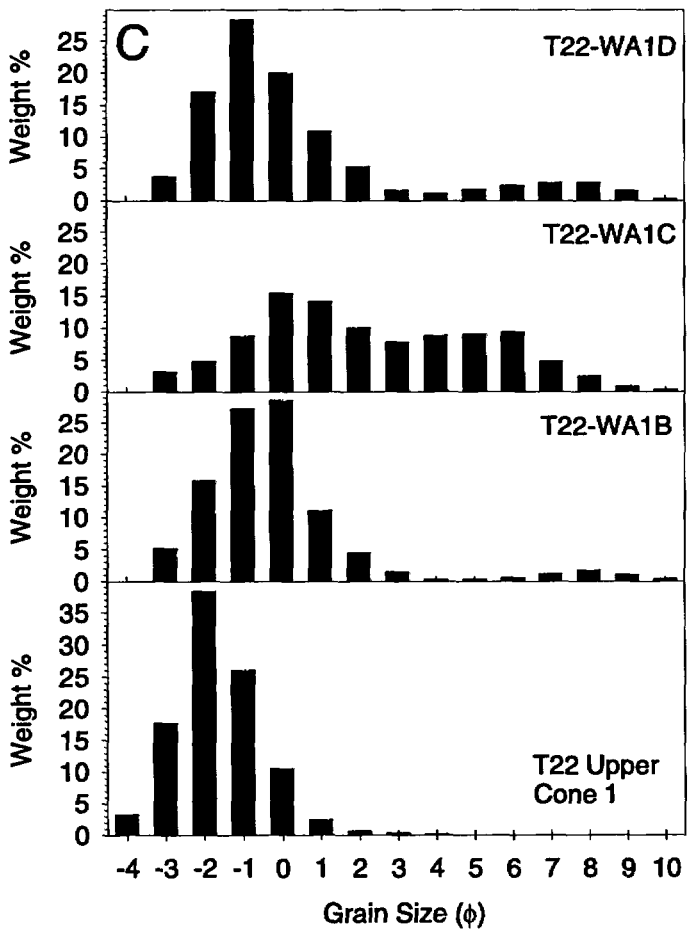

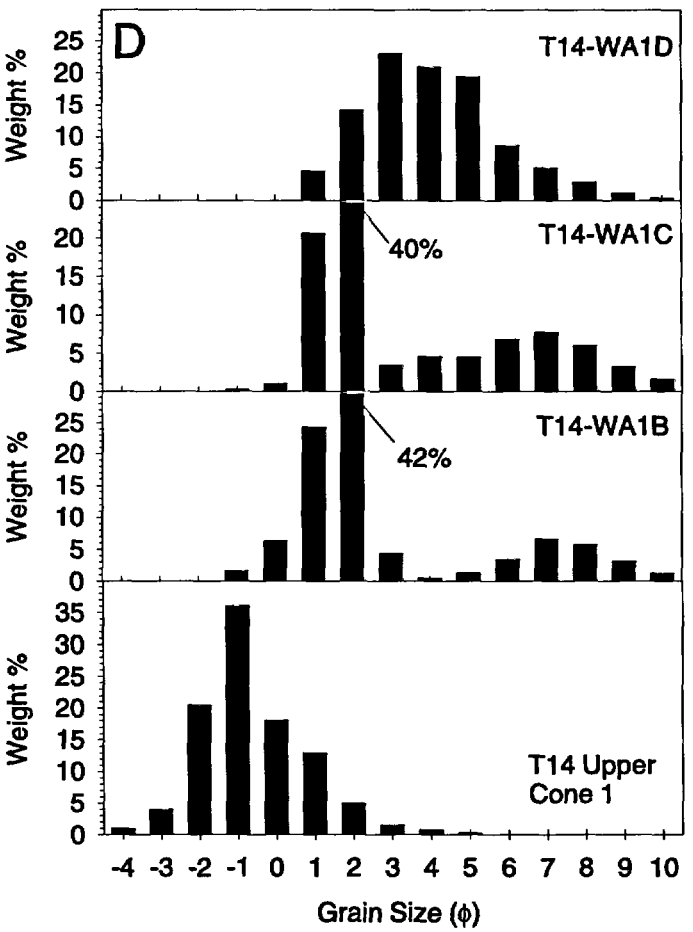

Doubik and Hill, Fig. 5

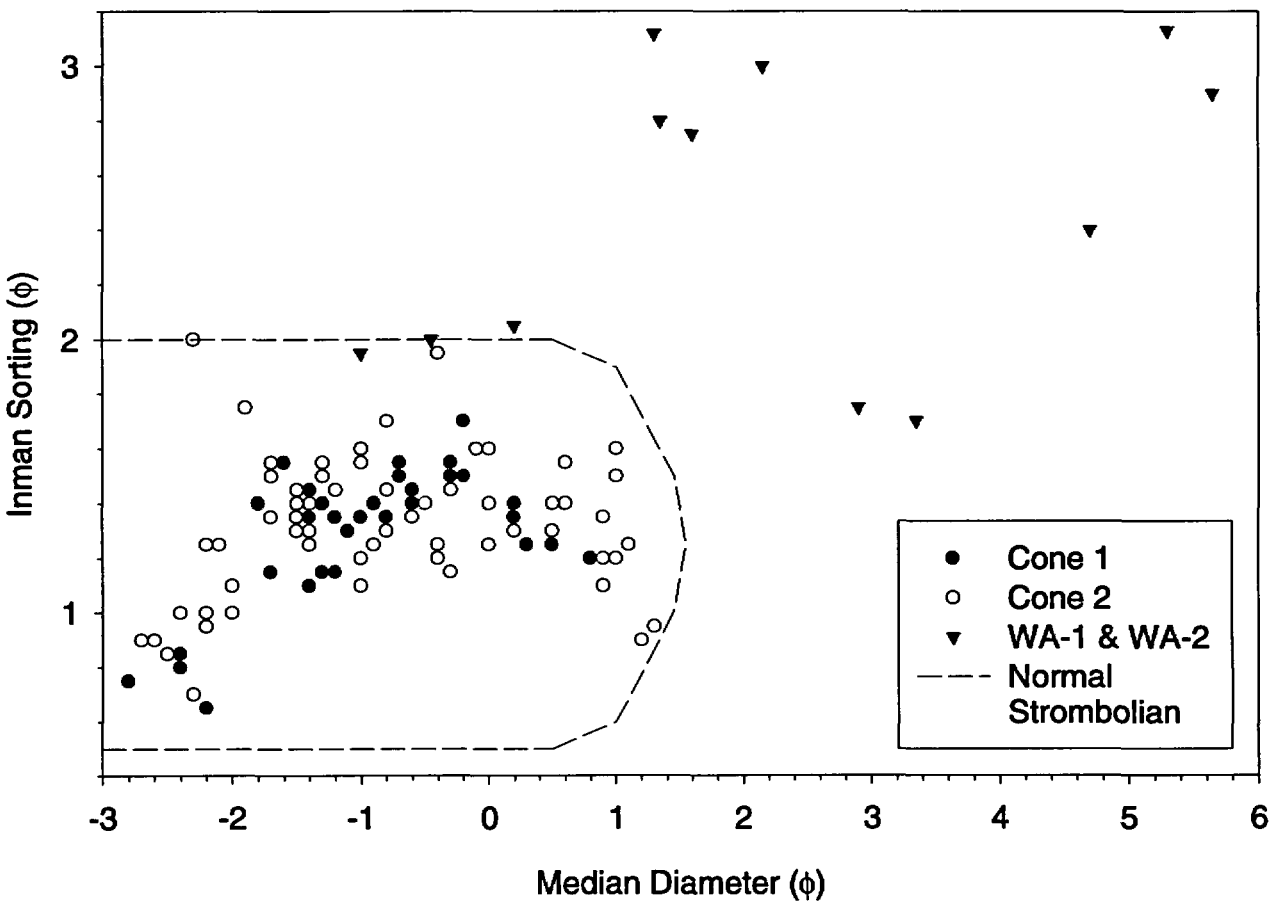

Doubik and Hill, Fig. 6

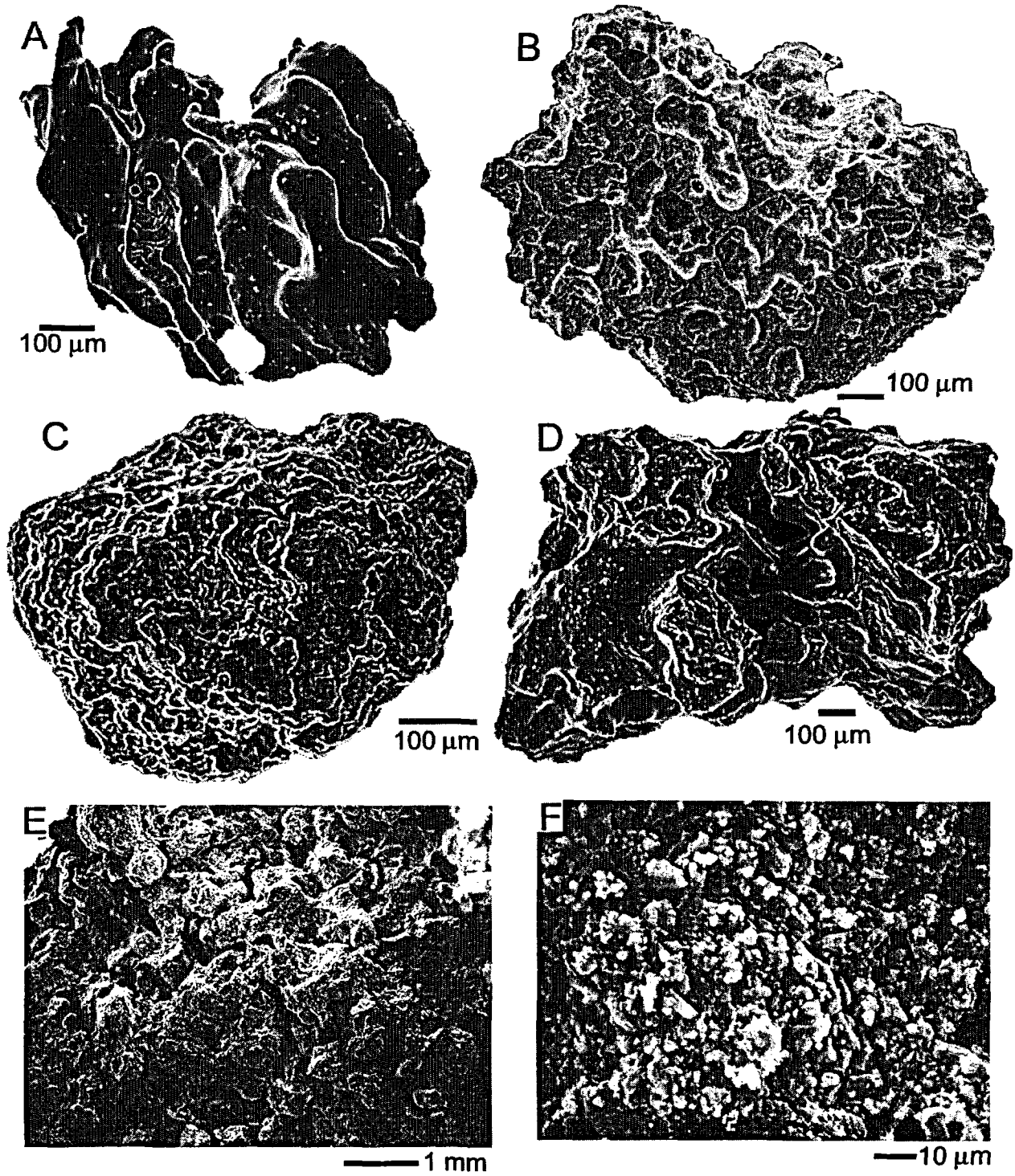

Doubik and Hill, Fig. 7

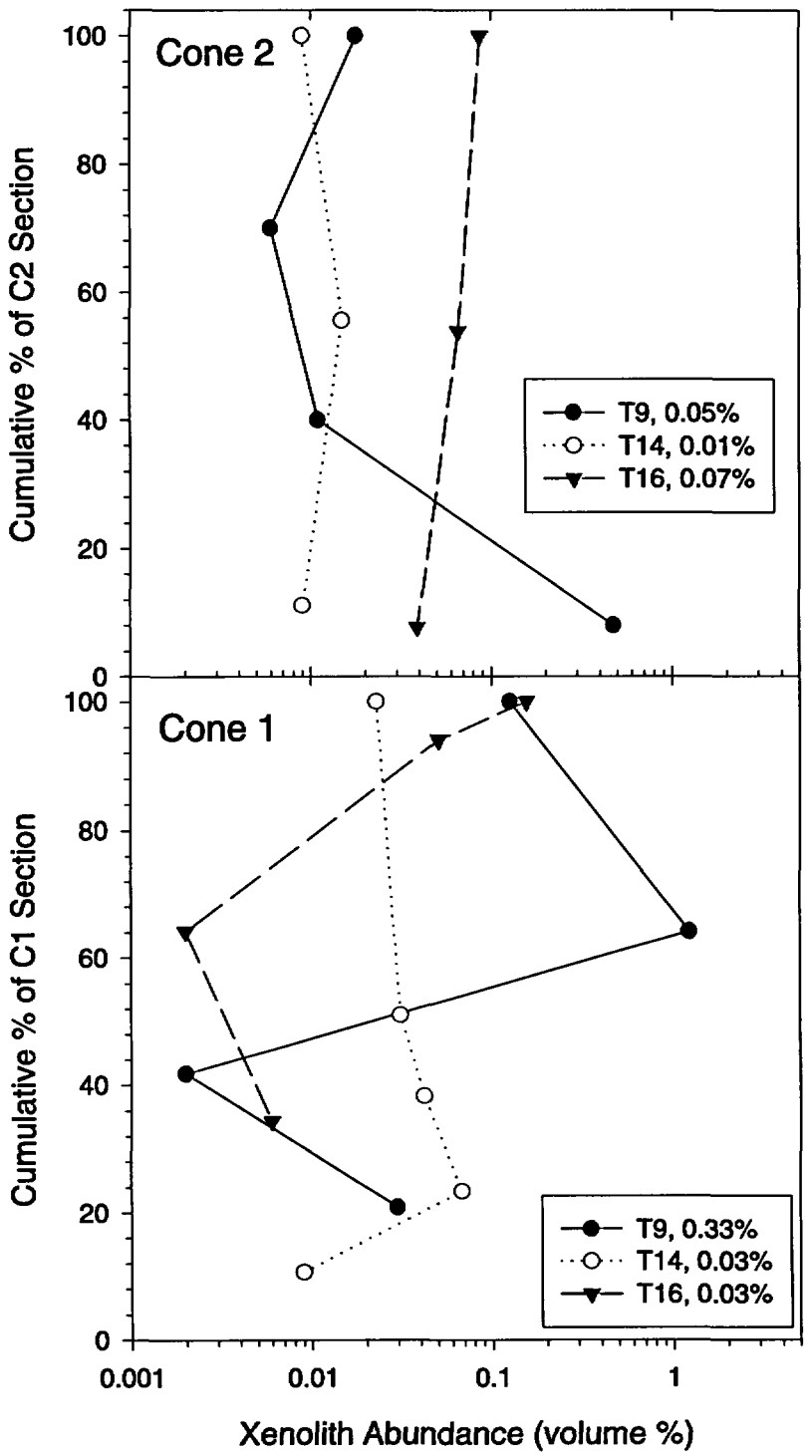

Doubik and Hill, Fig. 8

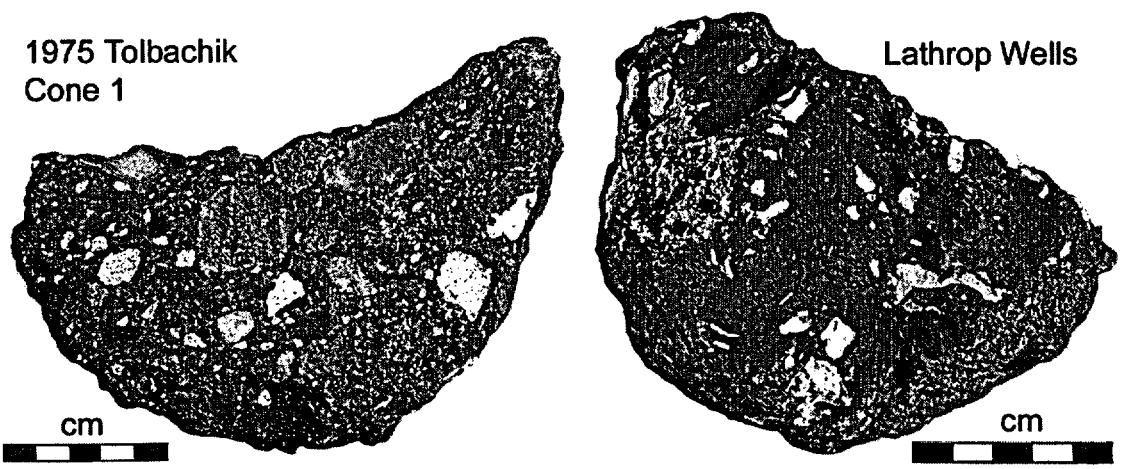

Doubik and Hill, Fig. 9

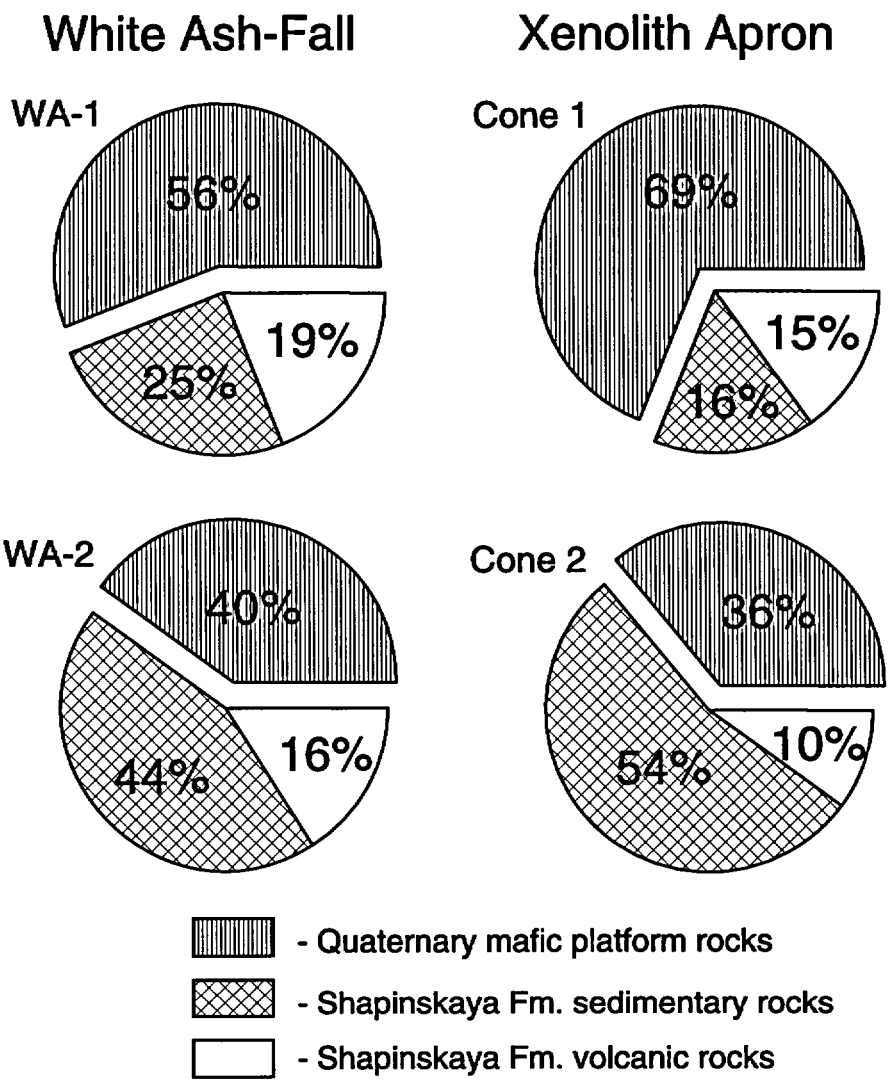

Doubik and Hill, Fig. 10

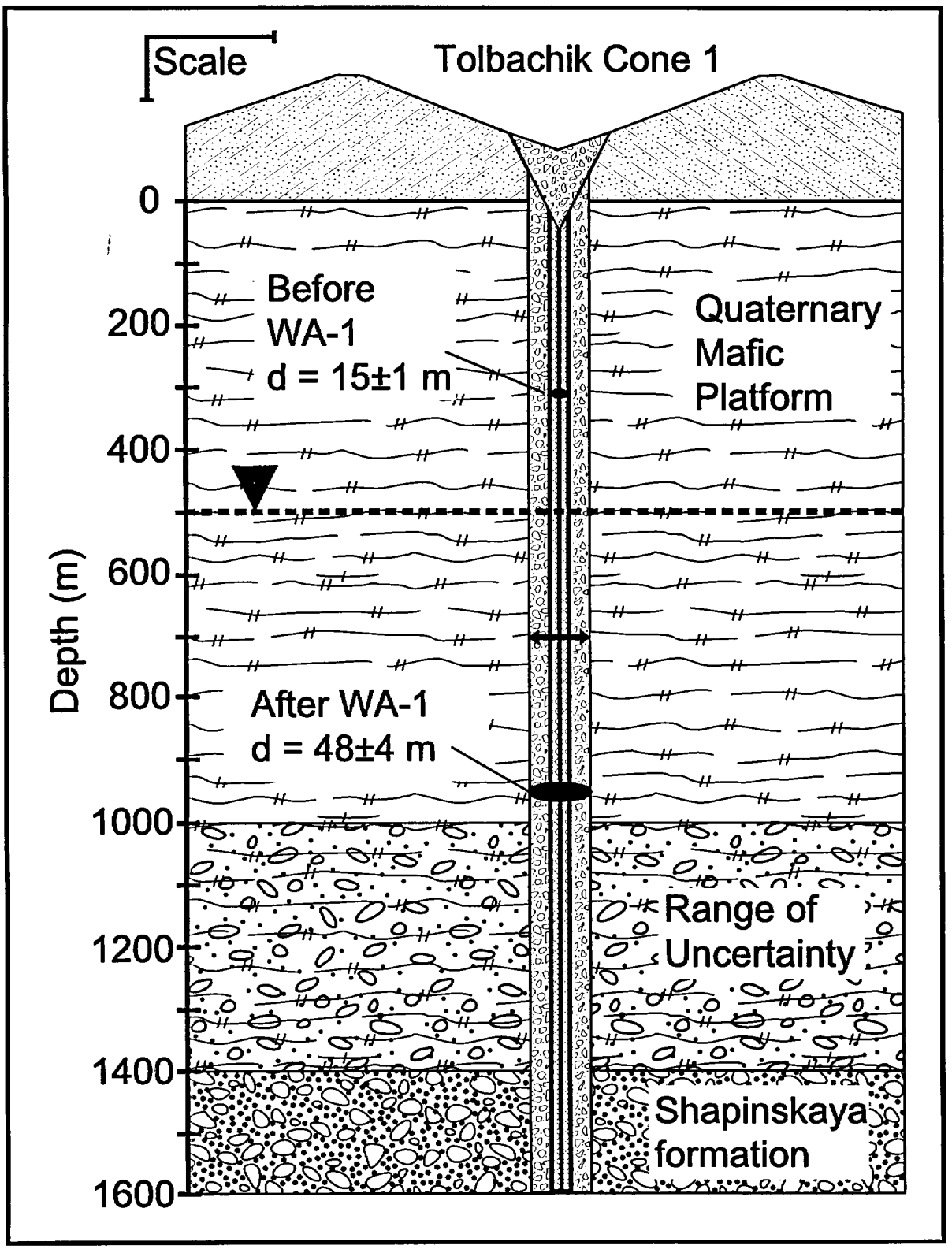

Doubik and Hill, Fig. 11